doi:10.1038/nature13993

Tel1^{ATM}-mediated interference suppresses clustered meiotic double-strand-break formation

Valerie Garcia[1], Stephen Gray[1], Rachal M. Allison[1], Tim J. Cooper[1] & Matthew J. Neale[1]

Meiotic recombination is a critical step in gametogenesis for many organisms, enabling the creation of genetically diverse haploid gametes. In each meiotic cell, recombination is initiated by numerous DNA double-strand breaks (DSBs) created by Spo11, the evolutionarily conserved topoisomerase-like protein[1], but how these DSBs are distributed relatively uniformly across the four chromatids that make up each chromosome pair is poorly understood. Here we employ *Saccharomyces cerevisiae* to demonstrate distance-dependent DSB interference in *cis* (in which the occurrence of a DSB suppresses adjacent DSB formation)—a process that is mediated by the conserved DNA damage response kinase, Tel1^{ATM}. The inhibitory function of Tel1 acts on a relatively local scale, while over large distances DSBs have a tendency to form independently of one another even in the presence of Tel1. Notably, over very short distances, loss of Tel1 activity causes DSBs to cluster within discrete zones of concerted DSB activity. Our observations support a hierarchical view of recombination initiation where Tel1^{ATM} prevents clusters of DSBs, and further suppresses DSBs within the surrounding chromosomal region. Such collective negative regulation will help to ensure that recombination events are dispersed evenly and arranged optimally for genetic exchange and efficient chromosome segregation.

We sought to elucidate the mechanisms that regulate the spatial patterning of meiotic DSBs. The conserved DNA damage response (DDR) kinase ataxia-telangiectasia mutated (ATM) inhibits excessive DSB formation in a number of organisms[2–5], suggesting that it might influence this process. While increased DSB formation in ATM mutants might arise from a loss of *trans*-interference[3,4] (between chromatids), or from global derepression of Spo11 catalytic activity, some observations in *S. cerevisiae*[6,7] can be explained by the loss of *cis*-interference[3,5] (within chromatids; see Supplementary Discussion for further details).

To test the idea that ATM activity functions in *cis* to suppress additional DSBs within broken chromosomes[3,5], we employed *S. cerevisiae* to assess the frequency with which four test chromosomes are cleaved multiple times in the presence and absence of Tel1 (the budding yeast orthologue of the human ATM protein) using strains that accumulate meiotic DSBs due to deletion of *DMC1*, the meiosis-specific RecA/Rad51 paralogue[8]. Fragmented chromosomes were separated by pulsed-field gel electrophoresis (PFGE) and detected with a probe positioned in the centre of each chromosome. Fragments shorter than the distance between the probe and the closest telomere must arise from at least two DSBs on the same chromatid. In line with our predictions, such molecules increased 1.3- to 1.7-fold upon deletion of *TEL1* (Fig. 1a, b and Extended Data Fig. 1a). Moreover, we noted a nonlinear inverse correlation between the fold-increase and the fragment length (Fig. 1c), which, because there were only minor increases in the apparent frequency of broken chromosomes as measured by indirect end-labelling (Fig. 1d and Extended Data Fig. 1b), cannot solely be explained by an increase in DSBs (Extended Data Fig. 2). These data instead suggest that the closer two DSBs are, the more likely that coincident cleavage is derepressed in the *tel1*Δ strain—as expected for loss of *cis*-interference.

DSB interference has not previously been demonstrated. To investigate further the idea that Tel1 mediates DSB interference, for each of the following analyses we compared the observed frequency of coincident DSB formation ('double-cuts') to that expected if DSBs were arising independently within the tested regions. We also used the ratio of these

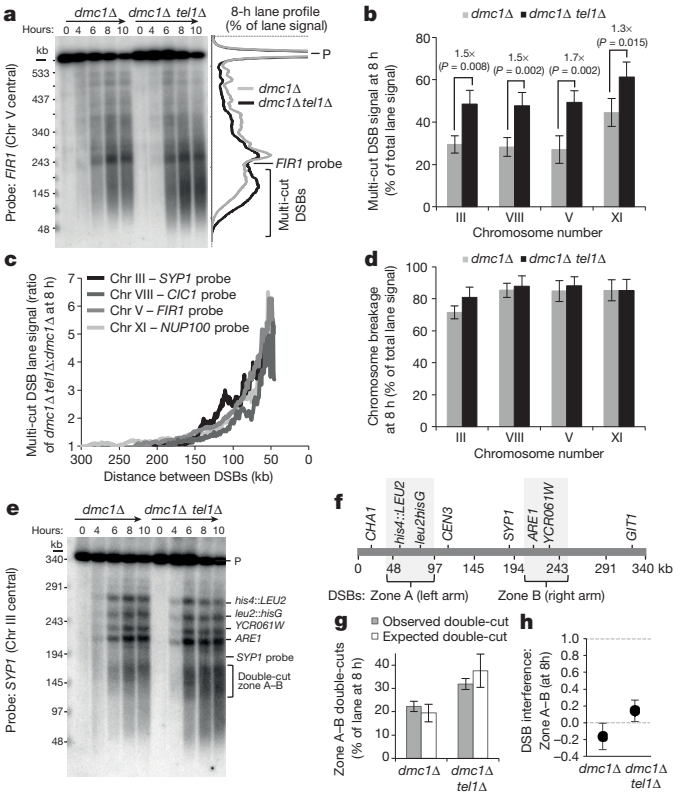

Figure 1 | Tel1 mediates distance-dependent suppression of DSB formation in *cis*. **a**, Agarose-embedded genomic DNA isolated at the indicated time points was fractionated by PFGE, transferred to nylon membrane and hybridized with a probe recognizing a central position on chromosome V. Example lane profiles depict the relative signal density for the 8-h time points. **b**, Quantification of multi-cut DSB signals, as depicted in **a**, for chromosomes III, VIII, V and XI (see Extended Data Fig. 1). Fold enrichment and statistical differences in average signal are indicated (*t*-test). **c**, Ratio of *dmc1*Δ *tel1*Δ versus *dmc1*Δ lane signal corresponding to multi-cut DSBs measured at 8 h (**a** and Extended Data Figs 1 and 2) plotted as a function of size. **d**, Average chromosome breakage for all four chromosomes (see Extended Data Fig. 1). **e**–**h**, Tel1-mediated DSB suppression spans less than 150 kb (see Extended Data Fig. 3 for details). **e**, As in **a** but hybridized with a probe recognizing a central position on chromosome III. Main DSB sites are indicated. 'Double-cut zone A–B': double-cuts formed from DSBs arising in both zones A and B on the same molecule. **f**, Physical map of chromosome III showing relative position of DSB zones and probes. **g**, Summary of observed and expected frequencies (based on independent events) of zone A–B double-cuts using data from 8 h time points. **h**, Calculated DSB interference between DSB zones A and B. **a**–**h**, Error bars, s.d. $n = 3$. *P* values, *t*-test.

[1]Genome Damage and Stability Centre, University of Sussex, Brighton BN1 9RQ, UK.

©2015 Macmillan Publishers Limited. All rights reserved

two values to calculate the strength of DSB interference between any two given DSB loci (see Methods). Positive values indicate strong DSB interference, whereas values close to zero indicate no DSB interference (that is, independence). Negative values indicate concerted DSB formation.

Long-range: the distribution of DSBs on chromosome III allowed us to assess whether DSBs separated by large distances (~150 kilobases) are subject to interference (Fig. 1e–h and Extended Data Fig. 3). In both *dmc1*Δ and *dmc1*Δ *tel1*Δ strains, the frequency of chromatids cut simultaneously within the major left-arm and right-arm DSB zones was very close to that expected for independent behaviour (Fig. 1g–h). We conclude that, at this large scale, DSB events arise independently of one another in the presence and in the absence of Tel1.

Medium range: we next probed the interval between two prominent Spo11-DSB hotspots separated by ~20 kb (the widely-characterized *HIS4*::*LEU2* hotspot[9] and a second site that maps within the *leu2*::*hisG* locus[1]; Fig. 2a,b). To improve signal detection we included a second recombination mutant (*sae2*Δ) which, owing to an inability to remove Spo11, accumulates DSBs without single-stranded DNA resection, causing DSB molecules to migrate as discrete double-stranded DNA bands[10–12]. In both *sae2*Δ and *dmc1*Δ cells, signals ranging from 16–60 kb—indicative of DSBs arising in the vicinity of *HIS4*::*LEU2* and the *leu2*::*hisG* region simultaneously (double-cuts)—although detectable, were present at frequencies significantly below those expected for independent cleavage within the two hotspot regions (that is, positive interference; Fig. 2b–d and Extended Data Fig. 4). By contrast, double-cutting increased in both strains upon *TEL1* deletion, arising at frequencies similar to those expected for independent cleavage (Fig. 2c), and indicating a loss of interference (Fig. 2d). By comparison, in both *sae2*Δ and *dmc1*Δ strains, upon downregulation of the *MEC1* (orthologue of the human *ATR* gene) branch of the DDR checkpoint pathway (achieved by deletion of *RAD24*, the orthologue of the human *RAD17* DDR clamp loader), double-cut frequencies remained lower than expected for independent DSB formation (Fig. 2c), suggesting that interference remained largely intact (Fig. 2d).

In *dmc1*Δ *tel1*Δ cells, although double-cut events plateaued after ~6 h (Extended Data Fig. 5a), they were first detectable at the earliest point that single DSBs were also detectable (2.5 h), suggesting that double-cuts do not arise from the accumulation of unrepaired DSBs in *dmc1*Δ and *sae2*Δ strains. Indeed, double-cuts were also readily detectable in the otherwise recombination-proficient *tel1*Δ single mutant (~1.2% of total lane signal)—a situation that was not observed in wild-type cells (Fig. 2e). Thus, over medium distances, Tel1 suppresses the formation of adjacent DSBs on the same chromatid in both recombination-deficient and recombination-proficient cells. *TEL1* deletion also caused coincident formation of DSBs separated by 10–70 kb at other genomic loci (Extended Data Fig. 5b). While the increase in double-cutting at these loci may partly be due to increased global DSB levels, our results collectively support the view that Tel1 mediates DSB interference in *cis* over domains spanning at least 70 kb, but that do not extend to 150 kb.

Short range: to investigate the role of Tel1 at closely-spaced DSBs we focused on the *HIS4*::*LEU2* locus, which consists of two strong DSB hotspots separated by only ~2.4 kb (Fig. 3a). Despite such spatial proximity, molecules of ~2.4 kb were visible in the *sae2*Δ single mutant (~0.35 ± 0.07% of lane signal)—indicative of simultaneous breakage at the two sites even in the presence of a functional *TEL1* pathway (Fig. 3b–d). Deletion of *TEL1* further increased the frequency of these molecules ~14-fold (4.71 ± 1.28% of lane signal). Such double-cut molecules were also detectable in the *tel1*Δ single mutant (~0.99 ± 0.19% of lane signal), albeit at appreciably lower signal intensity owing to the transient nature of DSBs in repair-proficient cells, and to ssDNA resection causing the DSB signals to migrate heterogeneously during electrophoresis, hampering detection (Fig. 3b–d). Double-cut molecules in wild-type cells were below the detection limit of our assays.

Surprisingly, both the *tel1*Δ and the *tel1*Δ *sae2*Δ strain displayed substantially greater levels of simultaneous Spo11-DSB formation than expected from the measured DSB frequencies at the two sites (Fig. 3d), a phenomenon referred to as negative interference (Fig. 3e). Furthermore, the two DSBs within *HIS4*::*LEU2* displayed no interference in the *sae2*Δ strain even though the suppressive Tel1 pathway is presumably active (Fig. 3d, e). Thus, in contrast to the more widely spaced DSB hotspots characterized above (medium-range), DSBs within *HIS4*::*LEU2* do not interfere, and actually appear to form concertedly in the absence of *TEL1*.

To investigate whether this phenomenon was unique to *HIS4*::*LEU2*, we measured the frequency of simultaneous cleavage arising between the natural *ARE1* hotspot and each of the many minor DSB sites that flank this locus (Fig. 4a, b). In absolute terms, loss of *TEL1* activity resulted in a 9.1-fold increase in the observed frequency of double-cutting across the *ARE1* locus (Extended Data Fig. 6a). We then calculated the strength of interference between the *ARE1* hotspot and each minor site using two methods to estimate the single-cut DSB frequencies: direct measurement using Southern blotting, and that calculated using three independent Spo11-oligo data sets (two from wild-type cells[1,13] and one from *tel1*Δ; S. Keeney and N. Mohibullah, personal communication; Fig. 4c, d,

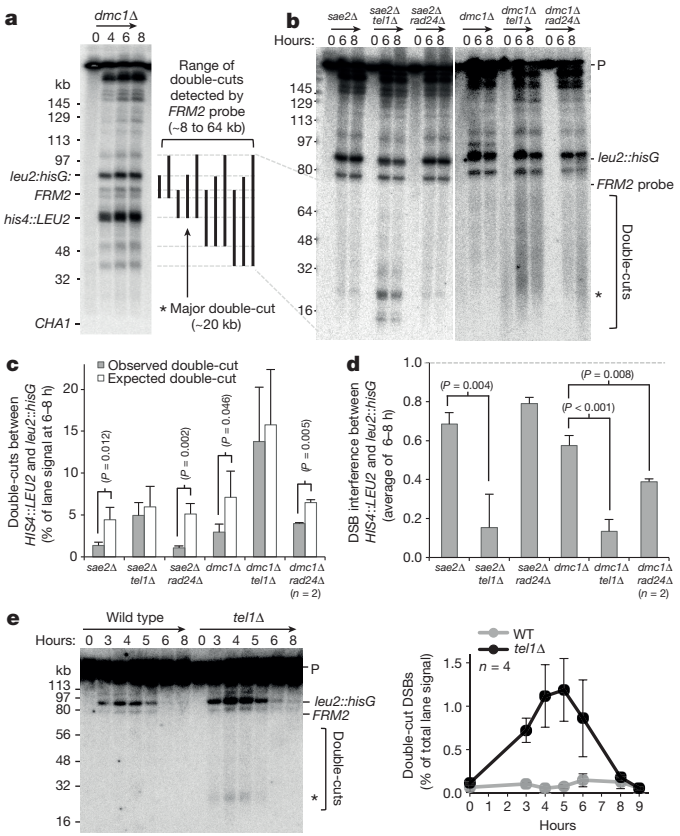

Figure 2 | Tel1 suppresses adjacent meiotic DSB formation within a 70-kb range. **a**, Example PFG with location of main DSBs (*HIS4*::*LEU2* and *leu2*::*hisG*) in left arm of chromosome III, detected by the *CHA1* probe, and diagram of the range of double-cuts detected by the *FRM2* probe in panels **b** and **e**. Major double-cut band is indicated with a star in **a**, **b**, **e**. **b**–**e**, Agarose-embedded genomic DNA isolated from the indicated time points and strains was fractionated by PFGE, transferred to nylon membrane and hybridized with *FRM2*. In *dmc1*Δ cells, the migration of the double-cut molecules was more variable and slightly retarded—at least in part owing to extensive ssDNA resection[25,26]. **c**, Quantification of observed (**b**) and expected double-cut frequencies. Expected frequencies of double-cut molecules (as if forming independently) were calculated from measured single-cut frequencies (Extended Data Fig. 4). Statistically significant differences are indicated. **d**, Calculated DSB interference between *HIS4*::*LEU2* and *leu2*::*hisG* (see Extended Data Fig. 4). **e**, Detection of double-cuts by PFGE as in **b** (left panel) and quantification of double-cuts (right panel) in the indicated strains. Error bars, s.d. $n = 3$, unless indicated. *P* values, *t*-test.

©2015 Macmillan Publishers Limited. All rights reserved

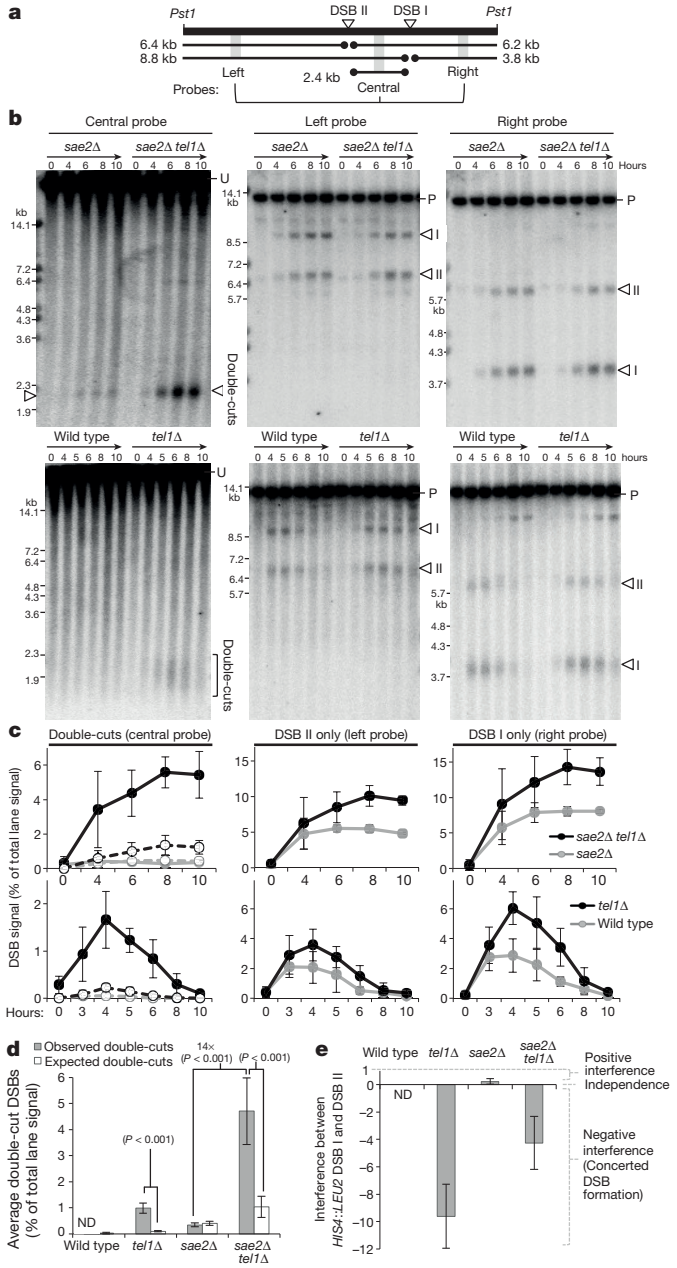

Figure 3 | Concerted DSB formation within the *HIS4*::*LEU2* hotspot. **a**, Diagram of *HIS4*::*LEU2* locus showing location of DSBs, fragment sizes and probes used. **b**, Genomic DNA isolated from the indicated time points and strains was fractionated by electrophoresis, transferred to nylon membrane and hybridized with probes as indicated. U, uncut parental DNA; P, PstI-digested parental DNA. DSB signals are marked with open triangles or bracket. **c**, Quantification of DSB and double-cut signals in **b**. Left panels, for comparison, expected double-cuts frequencies (dashed lines) are plotted alongside measured double-cut frequencies (plain lines). **d**, **e**, Summary chart of observed and expected (based on independent events) double-cuts (**d**) and interference values (**e**) calculated by averaging the 3–8 h (wild type and *tel1*Δ) or 4–10 h (*sae2*Δ and *sae2*Δ *tel1*Δ) time points from each repeat. Wild-type double-cut data were omitted from panels **c**–**e** because the signal was below our detection limit. ND, not determined. **a**–**e**, Error bars, s.d. $n = 4$. P values, t-test.

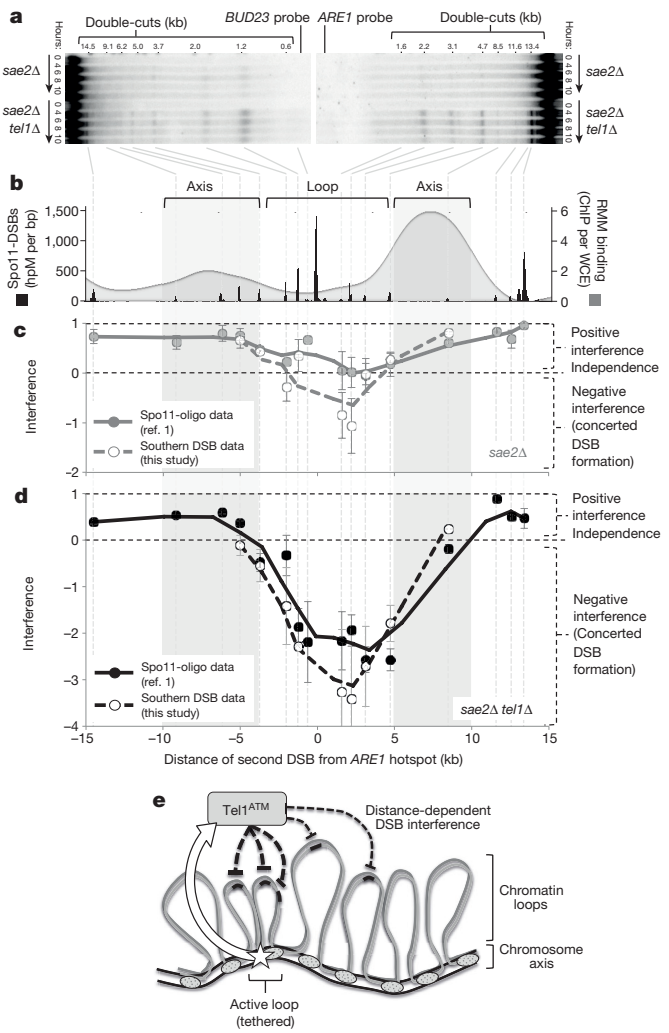

Figure 4 | Tel1 suppresses concerted DSB formation within chromatin loop domains. **a**, Genomic DNA isolated from the indicated time points and strains was fractionated by electrophoresis, transferred to nylon membrane and hybridized with either *BUD23* or *ARE1* probes. **b**, Diagram of *ARE1* locus ± 15 kb showing relative RMM binding profile[14] with Spo11-oligo (DSB) peaks overlaid[1]. ChIP/WCE, chromatin immunoprecipitation/input signal; hpM/bp, hits per million reads per base pair). Inferred chromosome axes and loop sites are highlighted. **c**, **d**, The frequency of each double-cut species in **a** was quantified, and interference between each pair of DSBs plotted after using the normalized frequency of Spo11-oligos[1] at each site to estimate expected frequencies of double-cutting (solid line, see Supplementary Methods), or the measured frequency of DSB formation obtained for a subset of sites from Southern blotting experiments (dashed line, Extended Data Fig. 6). Plotted points show averages ± standard deviation for two independent repeats (individual values within each repeat are averages of the 6–10 h time points). Plotted lines are 3-period moving averages. Comparable results were obtained when Spo11-oligo counts obtained from a second wild type[13] or a *tel1*Δ strain were used (S. Keeney and N. Mohibullah, personal communication). Comparison of observed and expected frequencies and statistical analyses are provided in Extended Data Fig. 6. **e**, Cartoon highlighting how Tel1^{ATM} suppresses DSB formation within (heavy dashed lines) and adjacent to (light dashed lines) active loop domains.

Extended Data Fig. 6, Methods, and data not shown). In the *sae2*Δ control, sites greater than 3–4 kb from *ARE1* displayed significant positive interference, whereas a zone of reduced DSB interference was observed for those DSBs in close proximity to *ARE1* (Fig. 4c and Extended Data Fig. 6). In the absence of *TEL1*, this differential effect was dramatically increased: cleavage of sites greater than 5 kb from *ARE1* arose at a similar frequency to that expected (that is, no interference), whereas DSB sites much closer to *ARE1* were disproportionately elevated, with observed double-cut frequencies being ~fourfold greater than expected if DSB formation was arising independently at each location (Fig. 4d and Extended Data Fig. 6). Collectively, we delimited a ~8 kb zone of strong negative DSB interference centred on the *ARE1* hotspot (Fig. 4d).

©2015 Macmillan Publishers Limited. All rights reserved

Our results suggest that the *ARE1* region is acting as a domain in which concerted DSB formation readily occurs, but which is to a large extent repressed by Tel1 activity. Recently a model for Spo11-DSB catalysis has gained favour in which short chromosomal domains, equal in size to individual chromatin loops, become tethered to the chromosome structural axis in order to trigger Spo11-DSB catalysis (the tethered loop–axis model[14,15]). We superimposed the binding position of chromosome axis components (Rec114, Mer2 and Mei4 (RMM) profile[14]) onto our map of simultaneous Spo11-DSB events and observed that the peak of negative DSB interference mapped to a trough in axis-protein binding signal—indicative of the centre of a chromatin loop (Fig. 4b, c). Such a correlation between regions of strong negative DSB interference and putative loop DNA was also observed at other tested loci, *YCRO61W*, *SRB2* and *CCT6* (Extended Data Fig. 7).

We propose that our observation of negative DSB interference at close range, apparently confined within a chromatin loop domain, is a previously unconsidered expectation of the tethered loop model. Specifically, loop-axis tethering of a specific region (to create a DSB-permissive subchromosomal domain) within only a subpopulation of cells will mean that population average measures of DSB frequency become underestimates of the DSB frequency within the tethered (active) fraction. Consequently, negative interference can be explained by loss of interference within a loop that is tethered in only a fraction of the population (Extended Data Fig. 8 and Supplementary Discussion for further details). While we favour this view, it is also possible that short-range concerted DSB formation is simply a consequence of DSBs being formed in regions of increased local DSB potential that are present in only a subpopulation of cells, and which map within chromosome loop domains (because that is primarily where DSBs occur) but are not caused by them.

In summary, our observations suggest that Tel1 mediates DSB interference in *cis* over domains that span ~100 kb, via a process that may be modulated by the unique organizational structure of the meiotic chromosome (Fig. 4e). Consequently, when Tel1 activity is lost, DSBs separated by medium-to-large distances (>10 kb) form independently of each other, whereas at close range (<10 kb), Tel1 suppresses DSB clustering within domains that may be defined by the boundary of local chromatin loops.

Whereas our work strongly indicates that Tel1 mediates DSB interference in *cis*, previous work concluded that Tel1 suppresses DSB formation in *trans*[4]. We propose that these apparently distinct inhibitory roles are simply two consequences of a single process: distance-dependent inhibition of DSB formation, which—owing to their close association—is transmitted along the pair of sister chromatids (that is, in *cis* and in *trans*; see Supplementary Discussion for further details and analysis). In mouse and flies, *ATM* mutants appear to undergo increased rates of recombination initiation, failed DSB repair, and apoptosis[2,3,16–18]. Our work predicts that these phenotypes may arise from an excess of DSBs within highly-localized active domains spanning a pair of sister chromatids[3].

Recent work suggested that, in budding yeast, Rec114 (an evolutionarily conserved axis-associated accessory protein required for Spo11-DSB formation[19]) is negatively regulated by Tel1-dependent phosphorylation[5]. The meiosis-specific chromosomal checkpoint adaptor protein, Hop1 (similar to mouse HORMAD1-2) and histone H2A are two other targets of Mec1/Tel1-mediated regulation[20,21]. However, double-cutting is not increased in strains harbouring non-phosphorylatable alleles of Rec114, Hop1 or H2A (V.G., R.M.A., M.J.N., unpublished observations), suggesting either that these factors act redundantly, or that DSB suppression is mediated via another target or function of Tel1.

Looking more broadly, our revelation that the strength of DSB interference varies non-uniformly with distance (Fig. 4) will have implications for the modelling of fine-scale recombination distributions in all sexually reproducing organisms, and particularly in mutants or under conditions that modulate ATM and ATR signalling. Furthermore, we note that clustered DSBs might behave as double-strand gaps—the initiators of recombination in the original model of DSB repair[22].

Our study also allows us to draw a parallel with the ATM-dependent repression of programmed DSB formation during antigen receptor chain *VDJ* recombination[23]. In both cases, potential cleavage sites are sequestered into active subdomains in which ATM activity suppresses concerted DSB formation[23]. It is interesting to consider whether similar mechanisms regulate other types of programmed, yet ostensibly stochastic, biological events—such as firing of DNA replication origins, a process itself regulated by the ATR kinase[24].

Online Content Methods, along with any additional Extended Data display items and Source Data, are available in the online version of the paper; references unique to these sections appear only in the online paper.

Received 25 March 2014; accepted 27 October 2014.
Published online 5 January 2015.

1. Pan, J. *et al.* A hierarchical combination of factors shapes the genome-wide topography of yeast meiotic recombination initiation. *Cell* **144,** 719–731 (2011).
2. Joyce, E. F. *et al. Drosophila* ATM and ATR have distinct activities in the regulation of meiotic DNA damage and repair. *J. Cell Biol.* **195,** 359–367 (2011).
3. Lange, J. *et al.* ATM controls meiotic double-strand-break formation. *Nature* **479,** 237–240 (2011).
4. Zhang, L., Kleckner, N. E., Storlazzi, A. & Kim, K. P. Meiotic double-strand breaks occur once per pair of (sister) chromatids and, via Mec1/ATR and Tel1/ATM, once per quartet of chromatids. *Proc. Natl Acad. Sci. USA* **108,** 20036–20041 (2011).
5. Carballo, J. A. *et al.* Budding yeast ATM/ATR control meiotic double-strand break (DSB) levels by down-regulating Rec114, an essential component of the DSB-machinery. *PLoS Genet.* **9,** e1003545 (2013).
6. Blitzblau, H. G. & Hochwagen, A. ATR/Mec1 prevents lethal meiotic recombination initiation on partially replicated chromosomes in budding yeast. *Elife* **2,** e00844 (2013).
7. Argunhan, B. *et al.* Direct and indirect control of the initiation of meiotic recombination by DNA damage checkpoint mechanisms in budding yeast. *PLoS ONE* **8,** e65875 (2013).
8. Bishop, D. K., Park, D., Xu, L. & Kleckner, N. DMC1: a meiosis-specific yeast homolog of *E. coli* recA required for recombination, synaptonemal complex formation, and cell cycle progression. *Cell* **69,** 439–456 (1992).
9. Cao, L., Alani, E. & Kleckner, N. A pathway for generation and processing of double-strand breaks during meiotic recombination in *S. cerevisiae. Cell* **61,** 1089–1101 (1990).
10. Keeney, S. & Kleckner, N. Covalent protein-DNA complexes at the 5′ strand termini of meiosis-specific double-strand breaks in yeast. *Proc. Natl Acad. Sci. USA* **92,** 11274–11278 (1995).
11. Prinz, S., Amon, A. & Klein, F. Isolation of COM1, a new gene required to complete meiotic double-strand break-induced recombination in *Saccharomyces cerevisiae. Genetics* **146,** 781–795 (1997).
12. McKee, A. H. & Kleckner, N. A general method for identifying recessive diploid-specific mutations in *Saccharomyces cerevisiae*, its application to the isolation of mutants blocked at intermediate stages of meiotic prophase and characterization of a new gene *SAE2*. *Genetics* **146,** 797–816 (1997).
13. Thacker, D., Mohibullah, N., Zhu, X. & Keeney, S. Homologue engagement controls meiotic DNA break number and distribution. *Nature* **510,** 241–246 (2014).
14. Panizza, S. *et al.* Spo11-accessory proteins link double-strand break sites to the chromosome axis in early meiotic recombination. *Cell* **146,** 372–383 (2011).
15. Blat, Y., Protacio, R. U., Hunter, N. & Kleckner, N. Physical and functional interactions among basic chromosome organizational features govern early steps of meiotic chiasma formation. *Cell* **111,** 791–802 (2002).
16. Barchi, M. *et al.* Surveillance of different recombination defects in mouse spermatocytes yields distinct responses despite elimination at an identical developmental stage. *Mol. Cell. Biol.* **25,** 7203–7215 (2005).
17. Di Giacomo, M. *et al.* Distinct DNA-damage-dependent and -independent responses drive the loss of oocytes in recombination-defective mouse mutants. *Proc. Natl Acad. Sci. USA* **102,** 737–742 (2005).
18. Barchi, M. *et al.* ATM promotes the obligate XY crossover and both crossover control and chromosome axis integrity on autosomes. *PLoS Genet.* **4,** e1000076 (2008).
19. Kumar, R., Bourbon, H. M. & de Massy, B. Functional conservation of Mei4 for meiotic DNA double-strand break formation from yeasts to mice. *Genes Dev.* **24,** 1266–1280 (2010).
20. Downs, J. A., Lowndes, N. F. & Jackson, S. P. A role for *Saccharomyces cerevisiae* histone H2A in DNA repair. *Nature* **408,** 1001–1004 (2000).
21. Carballo, J. A., Johnson, A. L., Sedgwick, S. G. & Cha, R. S. Phosphorylation of the axial element protein Hop1 by Mec1/Tel1 ensures meiotic interhomolog recombination. *Cell* **132,** 758–770 (2008).
22. Szostak, J. W., Orr-Weaver, T. L., Rothstein, R. J. & Stahl, F. W. The double-strand-break repair model for recombination. *Cell* **33,** 25–35 (1983).
23. Steinel, N. C. *et al.* The ataxia telangiectasia mutated kinase controls Igκ allelic exclusion by inhibiting secondary *Vκ*-to-*Jκ* rearrangements. *J. Exp. Med.* **210,** 233–239 (2013).
24. Toledo, L. I. *et al.* ATR prohibits replication catastrophe by preventing global exhaustion of RPA. *Cell* **155,** 1088–1103 (2013).

©2015 Macmillan Publishers Limited. All rights reserved

25. Westmoreland, J. *et al.* RAD50 is required for efficient initiation of resection and recombinational repair at random, gamma-induced double-strand break ends. *PLoS Genet.* **5,** e1000656 (2009).
26. Gray, S., Allison, R. M., Garcia, V., Goldman, A. S. & Neale, M. J. Positive regulation of meiotic DNA double-strand break formation by activation of the DNA damage checkpoint kinase Mec1(ATR). *Open Biol.* **3,** 130019 (2013).

Supplementary Information is available in the online version of the paper.

Acknowledgements V.G. was supported by an MRC New Investigator Grant to M.J.N. M.J.N. is supported by a University Research Fellowship from the Royal Society, a Career Development Award from the Human Frontiers Science Program Organisation, and a Consolidator Grant from the European Research Council. We thank S. Keeney and N. Mohibullah for sharing unpublished observations.

Author Contributions V.G. and M.J.N. designed the experiments, analysed the data and wrote the paper. V.G., R.M.A., S.G. and M.J.N. performed the experiments. T.J.C. provided data analysis, mathematical modelling and bioinformatics support.

Author Information Reprints and permissions information is available at www.nature.com/reprints. The authors declare no competing financial interests. Readers are welcome to comment on the online version of the paper. Correspondence and requests for materials should be addressed to M.J.N. (m.neale@sussex.ac.uk) or V.G. (v.garcia@sussex.ac.uk).

©2015 Macmillan Publishers Limited. All rights reserved

METHODS

Yeast strains and culture methods. Meiotic cultures were prepared as described[26]. Strains were derived from SK1 using standard techniques. *sae2*Δ, *exo1*Δ, *dmc1*Δ and *tel1*Δ are full replacements of the open reading frame with kanMX4 or hphNT2. A full strain list is provided in Extended Data Table 1.

Molecular techniques. DSB signals were detected via hybridization with specific DNA probes (detailed in Extended Data Table 2) after Southern blotting genomic DNA fractionated in agarose gels using standard techniques. For chromosome-scale analysis, genomic DNA was isolated in agarose plugs[26,27]. Radioactive signals were collected on phosphor screens, scanned with a Fuji FLA5100, and quantified using ImageGauge software.

DSB analysis by Southern blotting. Genomic DNA was isolated from aliquots of synchronously sporulating cultures as described previously[28] but with minor modifications. Briefly, spheroplasts were prepared in 1 M sorbitol, 0.1 M EDTA, 0.1 M NaHPO4 pH 7.5, 1% BME and 200 μg ml^{-1} zymolyase 100T for 1 h at 37 °C, and lysed by adding SDS to 0.5% and proteinase K to 200 μg ml^{-1} with incubation for 4 h to overnight at 60 °C. Protein was removed by mixing with an equal volume of phenol:chloroform:isoamyl alcohol (25:24:1), and nucleic acids precipitated by adding one-tenth volume of 3 M sodium acetate pH 5.2 and an equal volume of 100% ethanol. Precipitates were washed in 70% ethanol and dissolved in 1× TE overnight at 4 °C. RNase was added at 100 μg ml^{-1}, incubated for 60 min at 37 °C, genomic DNA was reprecipitated with ethanol/sodium acetate and DNA pellets were left to dissolve in 1× TE overnight at 4 °C. Signals were detected by Southern blotting of genomic DNA after fractionation on agarose gels as described previously[28].

For measuring the DSBs frequencies ('single-cuts') at various locations (for Figs 3, 4 and Extended Data Figs 6, 7), genomic DNA was digested with the appropriate restriction enzyme, fractionated on agarose in 1× TAE for ~18 h, transferred to nylon membrane under denaturing conditions, and hybridized with a probe allowing detection of DSBs to be quantified (as indicated in Extended Data Table 2).

For measuring the frequency of double-cuts (for Figs 3, 4 and Extended Data Figs 6, 7) undigested genomic DNA was fractionated and transferred using similar conditions. Membranes were hybridized with probes located between DSBs of interest (as indicated in figures and detailed in Extended Data Table 2).

Analysis of double-cutting at the *HIS4*::*LEU2* locus (Fig. 3) necessitated taking into account of the fact that the strains used in this study contain three copies of the *LEU2* gene: at the *his4X*::*LEU2*, *leu2*::*hisG* and *nuc1*::*LEU2* loci. Specifically, because the probe designed to detect double-cuts between sites I and II within the *his4X*::*LEU2* hotspot recognizes these three loci, numerous cross-reacting bands arise when probing DNA digested with restriction enzymes. Therefore undigested DNA was fractionated and transferred as for other loci. However, double-cut values recorded by this method were multiplied by three to correct for the fact that only ~1/3rd of the uncut parental DNA signal originated from the *HIS4*::*LEU2* locus. We note that double-cut frequencies measured using PstI-digested DNA were very similar to when using undigested DNA, but resulted in blots that were more complicated to analyse (data not shown). Radioactive signals were collected on phosphor screens, scanned with a Fuji FLA5100, and quantified (ImageGauge software, FujiFilm). Background subtraction was performed as described below.

DSB analysis by PFGE. DNA was prepared in agarose plugs as described[26,27]. For PFGE on Fig. 1 and Extended Data Figs 1 and 3, chromosomes were fractionated using a CHEF-DRIII PFGE system (Bio-Rad) using the following conditions: 1.3% agarose in 0.5× TBE; 14 °C; 6 V cm^{-1}; switch angle 120°; switch time of 20–60 s for 28 h. For PFGE on Fig. 2a, b and Extended Data Fig. 4, the following conditions were changed: switch time of 30 s for 3 h and 3–6 s for 37 h. For PFG on Fig. 2e and Extended Data Fig. 5: switch time of 30 s for 3 h and 3–6 s for 22 h. After transfer to nylon membrane under denaturing conditions[26,27], membranes were hybridized with DNA probes specific to: central, left and right sub-telomeric regions of four chromosomes (Fig. 1, Extended Data Figs 1 and 3); the *FRM2* region between *HIS4*::*LEU2* and *leu2*::*hisG* (Fig. 2 and Extended Data Figs 4 and 5a); or to regions between specific DSB sites on chromosome V (*POL5*), chromosome IX (*DOT5*), or chromosome III (*CTR86* and *YCR061W*) (Extended Data Fig. 5b). Probe details are listed in Extended Data Table 2. We note that due to small differences in the length of chromosome IX between otherwise isogenic isolates, DSB signals migrate at slightly different positions in the panel of strains in Extended Data Fig. 5. The positions of expected double-cuts are not affected by these differences, however, because the relative distance between each DSB is unaltered regardless of absolute chromosome length. Radioactive signals were collected on phosphor screens, scanned with a Fuji FLA5100, and quantified (ImageGauge software, FujiFilm). Background subtraction was performed as described below.

DSB and double-cut quantification. Radioactive signals were collected on phosphor screens, scanned with a Fuji FLA5100, and quantified using ImageGauge software. Background signal caused by exposure fogging and non-specific membrane background (based on vacant areas of the blot) was removed using linear subtraction. The contribution of sheared parental DNA to DSB and double-cut signal was removed using a gradient drawn along the lane profile starting from the base of the parental band down to the lane end. Signal above this cut-off were quantified as specific signal (DSBs or double-cuts). For quantification of double-cut molecules on membranes obtained from undigested DNA, signal that was retained in the wells (10–30% of the total lane signal) was added to, and treated as if it were, parental signal. This latter correction assumes that only parental DNA, and no double-cut DNA, is selectively retained in the well. In reality, some double-cut species probably do also get retained in the well, suggesting that our double-cut measurements may be slight underestimates.

Measurement of distance-dependent increases in multi-cut signal ratio. For Fig. 1c, for each chromosome, the signal intensity (expressed as a proportion of total lane signal) running through the multi-cut region (8 h time points from Extended Data Fig. 1a) of the *tel1*Δ *dmc1*Δ samples were each divided by the same signal obtained from the *dmc1*Δ control sample. The resulting ratio was plotted on the *y* axis against apparent double-cut length (in kb) on the *x* axis. The latter values were based on the approximate migration of the signal intensity on the PFG relative to lambda concatemer molecular weight markers. Due to the very low signal intensities towards the very bottom of the gels (and subsequently very erratic ratio calculations), the presented data was trimmed at ~50 kb. Double-cut signal length is indicative of the relative distance between any two given DSBs. Loss of Tel1 activity disproportionately increases the frequency of the shorter double-cut products (with little effect on fragments >100 kb), suggesting that Tel1 mediates distance-dependent DSB interference in *cis*. We note that owing to the fact that molecules with ssDNA regions migrate more slowly during PFGE[25] (that is, DSBs and double-cuts with resected DNA ends), the actual *x* axis (kb) values presented may be slight overestimates (perhaps +25%), and thus the distance that Tel1-dependent suppression is propagated may be somewhat shorter than the data make it appear.

To test whether the nonlinear increase in double-cutting frequency for shorter molecules could alternatively be explained by increases in DSB formation unassociated with any change in DSB interference, we developed a computer program that simulates DSB formation on a linear model of chromosome V (576 kb). This program was initially written in Sinclair BASIC using a plugin for the TextMate editor (http://macromates.com/) and the FUSE emulator for MacOSX (http://fuse-emulator.sourceforge.net/), and subsequently rewritten in MATLAB (http://www.mathworks.co.uk/). The simulation iterates 1 million times for each of the mean values of 2.5, 3, 3.5, and 4 DSBs per chromatid using DSB frequencies (per round of simulation) described by the Poisson distribution for the specified mean. To simulate the frequency distributions of fragments detected by an interstitial probe, tallies were made of only those fragments that include the simulated probe position (*FIR1* at position ~220 kb). Subsequently, ratios were calculated for each position within each of these simulated distributions and equivalent simulated distributions generated with mean DSB frequencies 1.5–4-fold greater. See Extended Data Fig. 2 for further details of our analysis. MATLAB code for this simulation is available on request.

Calculations of DSB interference. For calculations of interference between the left (zone A) and right (zone B) arm of chromosome III (Fig. 1e–h and as described in Extended Data Fig. 3), total DSB frequencies in each zone were measured using *CHA1* and *GIT1* probes, respectively. Expected frequencies of coincident cutting were obtained by multiplying these values. Observed frequencies of coincident cutting were estimated by measuring the total signal falling in a ~120–200 kb window (the approximate distance between zones A and B) after probing using the central, *SYP1* probe. Mean and standard deviation of the DSB frequencies for each time point are those of the three experimental repeats. A two-tailed *t*-test was used to compare the observed and expected samples. Although no time point showed statistically significant interference (neither positive nor negative), there were some notable trends: *dmc1*Δ cells display moderate negative interference at early time points, plateauing over time to display independence. Weak negative interference at early time points is actually expected, since at these time points, it is probable that only a subfraction of cells have initiated DSB formation, and thus expected double-cutting (calculated using the population average DSB frequency, which includes these inactive cells) will be an underestimate of that observed in the active fraction of cells. By contrast, *dmc1*Δ *tel1*Δ displays more positive interference than *dmc1*Δ $TEL1^{+}$, also increasing with time. Although this might seem counterintuitive compared to the rest of the *tel1*Δ observations made in this study, we believe it is an artefact of the analysis, and is explained by the fact that in *dmc1*Δ *tel1*Δ cells the frequency of additional DSBs in the central zone (creating the smeared 50–100 kb zone towards the bottom of the gel in Extended Data Fig. 3g) are moderately increased at all time points compared to *dmc1*Δ, thus potentially cutting the 'zone A–B double-cuts' into smaller fragments. As a result, our calculation of interference moderately underestimates the frequency of double-cutting in zone A and zone B simultaneously—and more so over time as total DSB frequency increases. Although not perfect in numerical value, we believe that these analyses are sufficient to

©2015 Macmillan Publishers Limited. All rights reserved

demonstrate that there is little or no measureable interference between zone A and zone B on chromosome III.

For calculations of interference between *HIS4*::*LEU2* and *leu2*::*hisG* (Fig. 2, and as described in Extended Data Fig. 4), total DSB frequency across the entire *HIS4*::*LEU2* locus (both DSB sites plus two telomere-proximal DSBs) and across the *leu2*::*hisG* and two flanking minor hotspots (within ~10 kb) were measured using PFGE in the various strains and the resulting values were multiplied to obtain an expected frequency of double-cutting (see Extended Data Fig. 4 for all calculations and statistical analysis). DSB frequencies for each repeat were averages of the 6–10 h time points, and the mean and standard deviation are those of the three experimental repeats. A two-tailed *t*-test was used to compare the observed and expected samples.

For calculations of interference between the two DSBs within the *HIS4*::*LEU2* locus (Fig. 3), double-cut signals derived from the central (*LEU2*) probe were multiplied by three to take into account that this probe hybridizes to three parental genomic locations (*HIS4*::*LEU2*, *leu2*::*hisG*, *nuc1*::*LEU2*). Expected frequencies of double-cutting were calculated by multiplying the frequency of DSB I and DSB II as measured using probes on the right and left of the hotspot respectively (Fig. 3c). An independent method to estimate double-cutting frequency, based on the observed difference in the frequency of DSB site I or site II when using left versus right probes, yielded similar values (also yielding negative interference), but appeared more prone to quantification error. Details of this method are available on request.

For calculations of interference across the *ARE1* locus (Fig. 4 and Extended Data Fig. 6), two methods were employed to calculate expected double-cut frequencies. Primarily, we converted Spo11 oligo counts[1] (reads per million; RPM) at individual DSB sites to % DSBs by normalizing to the *BUD23–ARE1* DSB signal measured by Southern blotting analysis, where *BUD23–ARE1* (2,721 RPM) = 8.37 ± 0.53% DSBs (*sae2*Δ) or = 13.2 ± 0.39% DSB (*sae2*Δ *tel1*Δ). Expected double-cut frequencies were then calculated by multiplying the frequencies of DSB formation at the test site and at the *ARE1* hotspot. Comparable DSB interference values were obtained when Spo11-oligo counts obtained from a second wild-type data set[13] were used, and when unpublished Spo11-oligo counts from a *tel1*Δ strain were used (data not shown; S. Keeney and N. Mohibullah, personal communication), indicating the degree of robustness of our analysis, and highlighting the fact that DSB frequencies vary relatively uniformly in the presence or absence of *TEL1*. Nevertheless, to independently confirm these findings, we used Southern blotting to directly measure the individual DSB frequencies at nine of the DSB sites that flank *ARE1* and calculated expected double-cut frequencies as above. This latter method, which in principle is more accurate because it directly assesses DSB frequency at each site using the same genomic DNA samples used to also measure observed double-cutting (and therefore precisely estimates expected double-cutting in *sae2*Δ and *sae2*Δ *tel1*Δ strains), produced results that agreed very well with the analysis using normalized Spo11-oligo data sets (see Fig. 4 and Extended Data Fig. 6 for a comparison). DSB and double-cut frequencies for each repeat were averages of the 6–10 h time points, and the mean and standard deviation are those of the three experimental repeats. A two-tailed *t*-test was used to compare the observed and expected samples.

In Extended Data Fig. 7, where possible we used Southern blotting to directly measure the individual DSB frequencies at each DSB site in *sae2*Δ and *sae2*Δ *tel1*Δ strains (using the average value across the 6–10 h time points), and used this value to calculate expected frequencies of double-cutting. However, there were a few DSB sites that were either below signal detection by Southern blotting, or that proved refractory to probes/digest combinations. For these sites we converted the reported Spo11-oligo counts[1] to % DSB frequency as follows:

For the analysis of interval A in Extended Data Fig. 7d–f, the frequency of Spo11-oligos at the *BRL1–PUT2* locus (138 RPM) was converted to an estimated DSB frequency of 0.38 ± 0.03% in *sae2*Δ and 0.41 ± 0.03% in *sae2*Δ *tel1*Δ based on normalizing the frequency of Spo11-oligos at the main *SRB2–NCP1* hotspot (3,639 RPM) to 10.01 ± 0.76% DSBs (*sae2*Δ) or 10.8 ± 0.68% DSBs (*sae2*Δ *tel1*Δ) following direct measurement of DSB formation at the *SRB2–NCP1* hotspot using Southern analysis.

For the analysis of intervals B, C, and D in Extended Data Fig. 7g–i, the frequency of Spo11-oligos at the respective loci (177 RPM, 169 RPM, and 400 RPM) were converted to estimated DSB frequencies of 0.63%, 0.60%, and 1.42% in *sae2*Δ and 0.83%, 0.79%, and 1.87% in *sae2*Δ *tel1*Δ based on normalizing the frequency of Spo11-oligos at the main *YDR186C–CCT6* hotspot (3,997 RPM) to 14.15% DSBs (*sae2*Δ) or 18.72% DSBs (*sae2*Δ *tel1*Δ) following direct measurement of DSB formation at the *YDR186C–CCT6* hotspot using Southern analysis.

Potential caveats with double-cut quantification using the methods described. Our high-resolution analysis of interference in Fig. 4, Extended Data Figs 6, 7 assesses the frequency of coincident DSB formation at any pair of tested DSB sites (double-cuts) compared to the frequency of expected coincident cutting calculated by multiplying the measured single cut DSB frequencies at the pair of sites being tested. On any given side of a strong hotspot, double-cuts of increasing length are measured using the same probe (anchored close to a major DSB hotspot). A caveat of this method is that as the second site becomes more distant from the first (the anchor point), the ability to detect the assayed double-cut product will be impeded by the presence of any intervening additional DSB. However, for the genomic loci we have investigated, this small systematic error will have minimal impact on our data collection, as explained in detail below.

Given a molecule with DSBs arranged in linear order: A, B, C. If all DSBs form independently, the likelihood of an intervening DSB "B" cutting a molecule that has already been cut at site A and C, is directly proportional to the frequency of DSB formation at "B". If DSB B = 5%, the observed frequency of A–C double-cuts will actually be only 95% of its actual value (5% of the time it is cut by B). Thus the corrected frequency of double-cut A–C is obtained by dividing the observed value by 0.95 (= multiplied by 1.053). Note that many interstitial DSBs are far weaker than 5%, and therefore will have an even lesser effect (see Extended Data Fig. 6 column D and N for examples of DSB frequencies across the *ARE1* locus). This means that larger double-cuts are only very weakly underestimated (unless the sum of all the intervening cuts is very large, which in general is not true; see comment earlier). Even if we were to attempt to correct for this systematic error, it would result in only a subtle increase in the frequency of double-cuts in the larger range, resulting in a slightly wider and stronger spread of reduced/negative interference in *tel1*Δ. Note that this correction will not fundamentally change our observation that negative interference is centred within a loop.

Alternatively, if DSBs are forming concertedly (as we propose occurs in loop domains), then the frequency that A–C is cut by B is not proportional to the population average frequency of DSBs at B, but instead, A–C will be cut at whatever frequency B cuts in situations when A (and/or C) are activated. In this scenario, A–C might be more severely underestimated. As above, while this might result in a pattern of negative interference that spreads more broadly and more strongly than depicted in Fig. 4, it again will not change the observation of negative interference in the loop. Moreover, if negative interference is indeed restricted to loops (as we propose in this manuscript), the apparently disproportionate underestimate in double-cuts due to intervening DSBs will only be true of DSBs within the activated region. Outside of this concerted region, we would expect DSBs to behave independently (and have less impact, as above).

We note that using both correction methods (independent DSBs or concerted DSBs) will actually strengthen the phenomenon of negative interference that we observe in the absence of *TEL1*. Our small underestimate of double-cutting might also explain why weak interference is still retained over moderate ranges (>10 kb) even in the absence of *TEL1* (that is, such weak interference that remains may be due to moderately underestimating long double-cuts, rather than actual retained interference; observed in both Fig. 2d and Fig. 4d).

Bioinformatics. Raw Spo11-oligo data sets[1] containing signals at 1-bp step sizes were smoothed via Hann windows of varying size and zero values were filtered/removed to reduce file size via grep commands. Mei4-HA, Mer2-HA and Rec114-HA ChIP/WCE signals (sampled at $t = 4$ h and normalized by the authors[14]) were averaged with equal weighting and a continuous and smoothed data set was constructed via spline interpolation on MATLAB R2013+. Resulting data sets were exported directly into .bedGraph files and additional .BigWig files were created via the precompiled UCSC bedGraphToBigWig tool.

27. Murakami, H., Borde, V., Nicolas, A. & Keeney, S. Gel electrophoresis assays for analyzing DNA double-strand breaks in *Saccharomyces cerevisiae* at various spatial resolutions. *Methods Mol. Biol.* **557,** 117–142 (2009).
28. Garcia, V., Phelps, S. E., Gray, S. & Neale, M. J. Bidirectional resection of DNA double-strand breaks by Mre11 and Exo1. *Nature* **479,** 241–244 (2011).

©2015 Macmillan Publishers Limited. All rights reserved

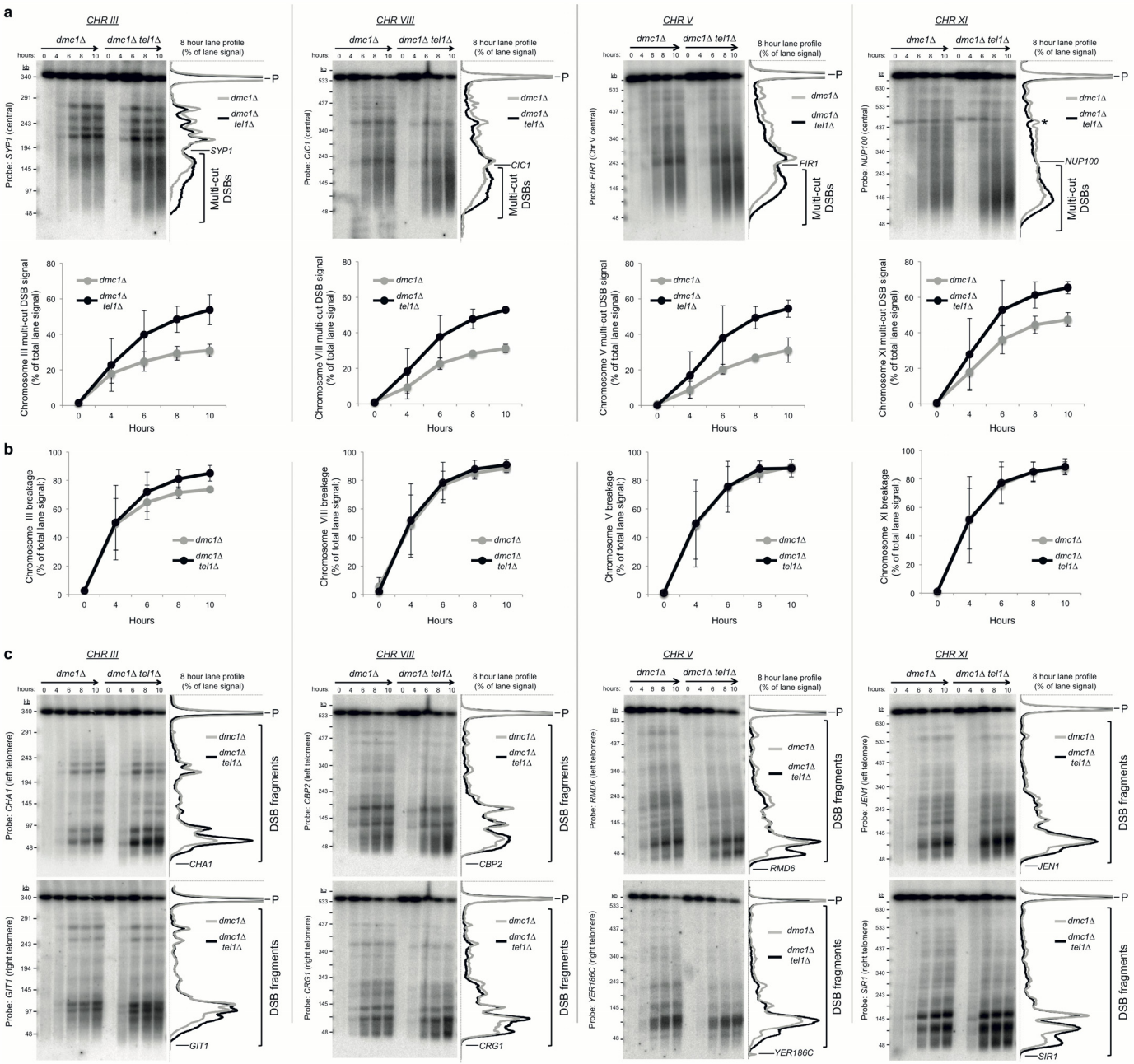

Extended Data Figure 1 | Tel1 suppresses the formation of multiple DSBs on the same chromatid. **a**, Top: agarose-embedded genomic DNA isolated at the indicated time points was fractionated by PFGE, transferred to nylon membrane and hybridized with probes recognizing a central position on chromosome III, VIII, V and XI. Example lane profiles depict the relative signal density for the 8 h time points. Representative blots are shown. Areas defined for quantification of multi-cut DSBs (bottom panel) are indicated. Asterisk: cross-hybridization band. **b**, Quantification of total chromosome breakage measured in **a**. **c**, As in **a** but using probes specific to the left (top panel), or right (bottom panel) telomere. In agreement with more DSBs per chromatid being formed in the absence of Tel1, close inspection of the PFGE lane profiles revealed that *dmc1*Δ *tel1*Δ cells had an increased frequency of shorter chromosome fragments, yet also fewer large chromosome fragments. Because a similar shift in DSB distribution towards shorter molecules is also observed when chromosomes are probed from their opposite end (compare top and bottom panels), this apparent shift can be explained by an increase in the frequency of multiple DSBs arising on the same chromatid in *dmc1*Δ *tel1*Δ relative to *dmc1*Δ. **a**–**c**, Error bars, s.d. $n = 3$.

©2015 Macmillan Publishers Limited. All rights reserved

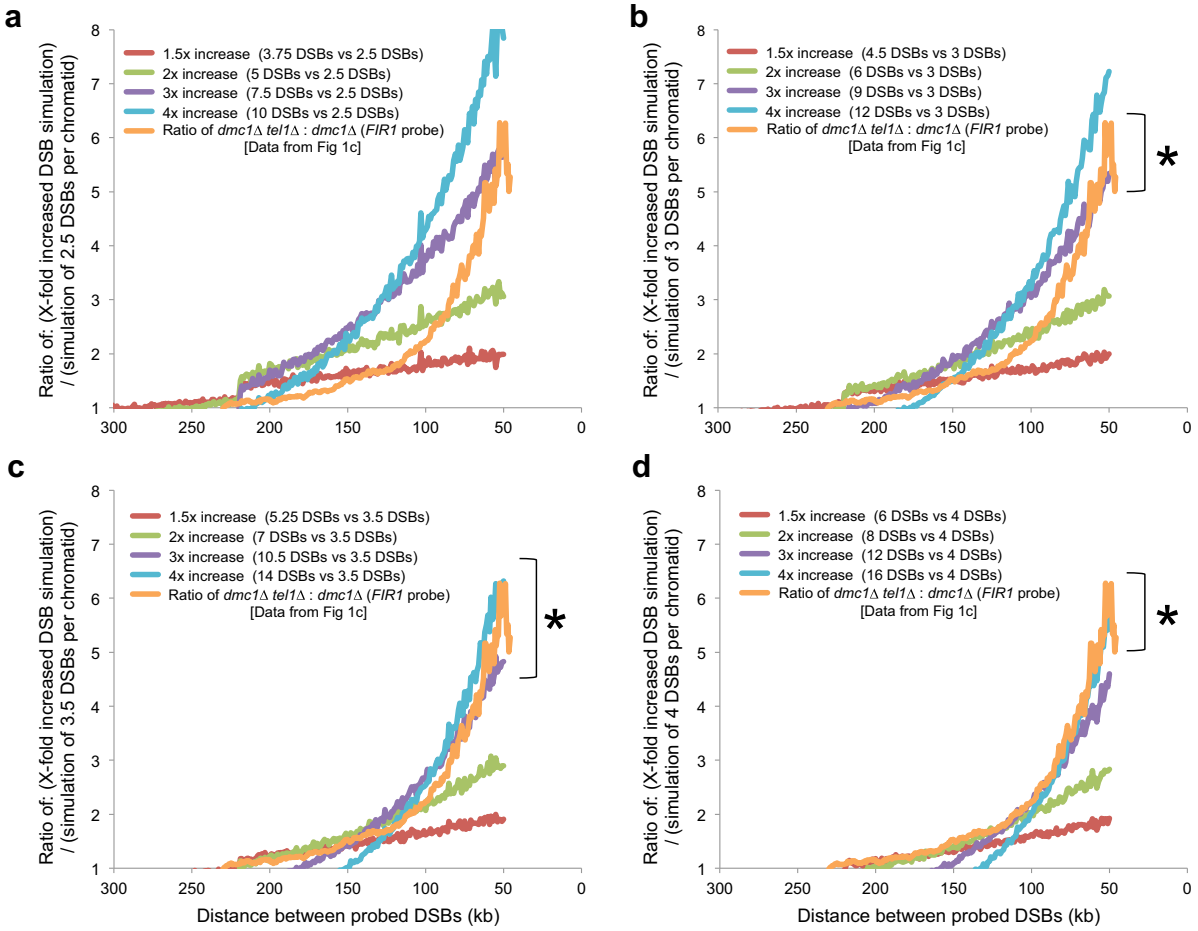

Extended Data Figure 2 | Nonlinear increases in the frequency of closely spaced DSBs that arise upon *TEL1* deletion cannot be explained by increases in absolute DSB frequency. a–d, To test whether the nonlinear increase in double-cutting frequency for shorter molecules (Fig. 1c) could alternatively be explained by increases in DSB formation unassociated with any change in DSB interference, DSB formation on chromosome V (576 kb) was simulated 1 million times for each of the mean values of 2.5, 3, 3.5 and 4 DSBs per chromatid using DSB frequencies (per round of simulation) described by the Poisson distribution for the specified mean. These frequencies are approximately equivalent to 217, 260, 304 and 347 DSBs per cell (~50 Mb). To simulate the frequency distributions of fragments detected by an interstitial probe, tallies were made of only those fragments that include the simulated probe position (*FIR1* at position ~220 kb). Subsequently, ratios were calculated for each position within each of these simulated distributions and equivalent simulated distributions generated with mean DSB frequencies 1.5× (red), 2× (green), 3× (purple), and 4× (blue) greater than the baseline. Finally, these data simulations were overlaid with the experimental observations made from chromosome V using the *FIR1* probe when comparing the ratio of the *dmc1*Δ *tel1*Δ: *dmc1*Δ (data from Fig. 1c; orange). In all cases, as in Fig. 1c, data has been trimmed for fragments shorter than 50 kb and greater than 300 kb. The asterisks indicate instances of similarity between simulated and observed patterns. We note that in no circumstances do the simulations match the steep nonlinear curve, which is a hallmark of the experimental data caused by *TEL1* deletion. The closest match is arguably simulating the ratio between a starting mean DSB frequency of 3.5 and that obtained from a 3–4-fold increase (**c**). While these simulations create a potential match, they both require the relatively high initial frequency of DSB formation in *dmc1*Δ cells of 304 DSBs per cell (note that the wild-type average frequency is estimated at ~160 DSBs per cell[1]), increasing to 900–1,200 DSBs per cell upon *TEL1* deletion. Moreover, in accord with the increased DSB frequency per cell, site-specific DSB frequencies would increase 3–4-fold in *dmc1*Δ *tel1*Δ cells relative to *dmc1*Δ cells to fit this simulation, something that we do not observe: average fold-changes in both *sae2*Δ and *dmc1*Δ strains are only ~1.5× upon *TEL1* deletion (Fig. 3c, Extended Data Fig. 4c and Extended Data Fig. 6a), a fold-change that is modelled by each of the red plots—all of which show very poor correlations with the observed data. Thus we conclude that the nonlinear inverse correlation between the fold-increase and the inter-DSB fragment length cannot solely arise from a global increase in DSB formation, but rather because the closer two DSBs are, the more likely that coincident cleavage is derepressed in the *tel1*Δ strain—as expected for a loss of *cis*-interference.

©2015 Macmillan Publishers Limited. All rights reserved

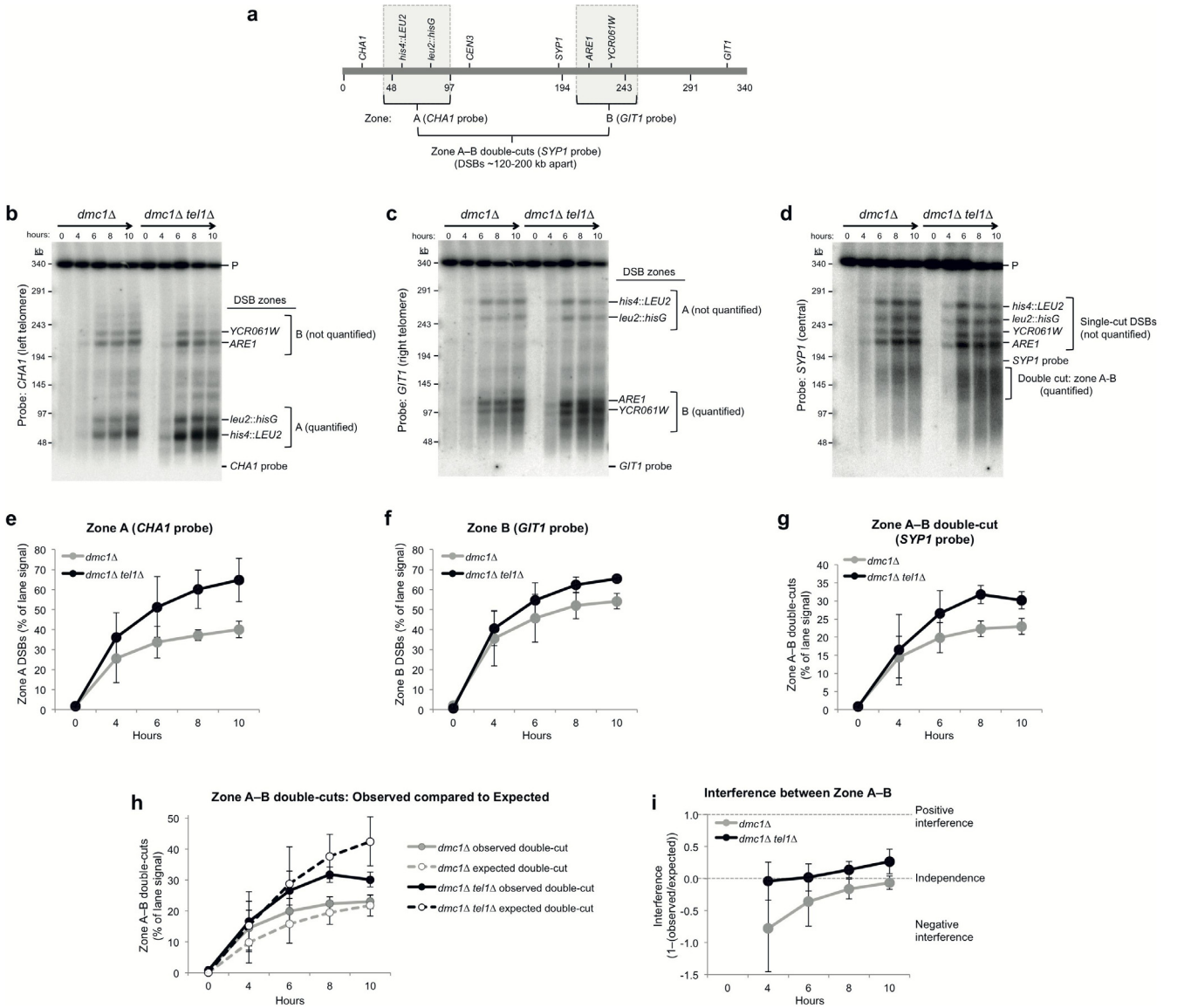

Extended Data Figure 3 | Tel1-mediated DSB interference spans less than 150 kb. **a**, Physical map of chromosome III showing relative position of DSB zones and probes. **b**, **d**, Agarose-embedded genomic DNA isolated at the indicated time points was fractionated by PFGE, transferred to nylon membrane and hybridized with probes recognizing a left (**b**), right (**c**) or central position (**d**) on chromosome III. Probes, main DSB sites and areas selected for quantification of DSBs arising in individual zones are indicated. **e**–**g**, Quantification of DSB formation in zone A (**e**), zone B (**f**) and double-cuts arising from DSBs occurring in both A and B on the same molecule (**g**). **h**, Comparison of observed zone A-B double-cuts (**g**) to expected zone A-B double-cuts (calculated from single cut frequencies measured in **e**, **f**). We observe no statistical difference between observed and expected values at any time point (*t*-test: *P* values all above 0.25 except *dmc1*Δ *tel1*Δ $t = 10$ h sample, 0.061). **i**, Calculated DSB interference between DSB zones A and B. **b**–**i**, Error bars, s.d. $n = 3$. See Supplementary Discussion for further details of this analysis.

©2015 Macmillan Publishers Limited. All rights reserved

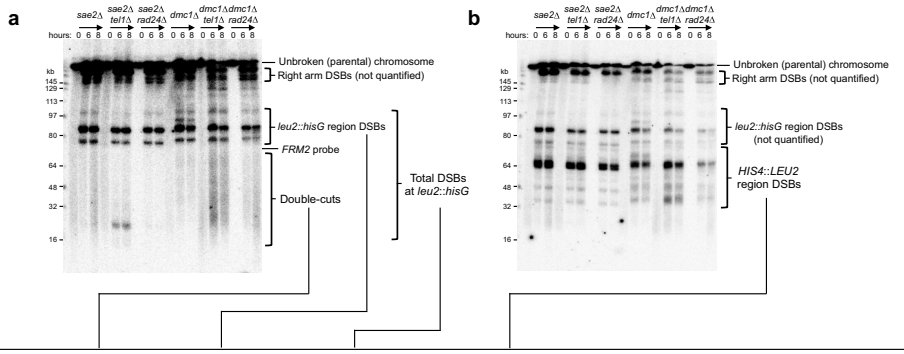

c

	Column	A	B	C	D	E	F	G	H	J	K	L	M	N	P	Q	R
		Double cuts observed		*leu2::hisG* region DSBs		Total *leu2::hisG* region DSBs (A + C)		*HIS4::LEU2* region DSBs		Double-cuts Expected (E x G)		Interference (1–(A /J))		Statistics (T test)		Statistics (T test)	
	Probe:	*FRM2*		*FRM2*		*FRM2*		*CHA1*		Expected				Test: Observed is less than Expected? (A<J)		Test: Interference is less than control? (L<L')	
Strain	Repeats (n)	Average	STDEV	Average	STDEV	Average	STDEV	Average	STDEV	Average	STDEV	Average	STDEV	P-value	Significant?	P-value	Significant?
sae2Δ	3	1.37	0.40	16.04	2.74	17.40	3.09	25.07	4.33	4.45	1.47	0.68	0.06	0.012	Yes		
sae2Δ tel1Δ	3	4.93	1.54	13.94	3.94	18.87	4.72	31.28	5.92	6.00	2.40	0.15	0.17	0.277	No	0.004	Yes
sae2Δ rad24Δ	3	1.07	0.22	17.65	2.57	18.72	2.62	27.33	3.94	5.14	1.24	0.79	0.03	0.002	Yes	0.026	No (increased)
dmc1Δ	3	2.93	0.98	20.27	5.41	23.20	6.39	29.74	5.45	7.12	3.15	0.58	0.05	0.046	Yes		
dmc1Δ tel1Δ	3	13.78	6.51	21.25	2.79	35.02	8.80	43.57	8.40	15.75	6.64	0.13	0.06	0.366	No	0.000	Yes
dmc1Δ rad24Δ	2	3.97	0.11	16.31	1.95	20.28	2.06	32.55	1.35	6.50	0.33	0.39	0.01	0.005	Yes	0.008	Yes

Notes:
A-R: Column identifiers
A, C, E, G, J: Values are expressed as a percentage of total DNA. For each repeat, each measurement is an average of the 6 and 8 hour timepoint.
A: Double-cuts detected by *FRM2* probe are of variable length (~8-64 kb) depending which specific DSBs break within the *HIS4::LEU2* and *leu2::hisG* regions.
The major band at ~20 kb arises from double-cuts between the major hotspots within *HIS4::LEU2* (at position 66 kb) and *leu2::hisG* (at position 86 kb) as shown in panel b.
C: The *FRM2* probe is useful to estimate the frequency of DSBs in the *leu2::hisG* region, but will underestimate this value when a DSB forms telomere-proximal to the probe (i.e. at *HIS4::LEU2*) in the same molecule.
Thus total DSB formation in the *leu2::hisG* region can be calculated by adding the frequency of double-cuts (between *leu2::hisG* and *HIS4::LEU2*) to the measured *leu2::hisG* signal (E).
J: Expected frequency of double-cuts is calculated by multiplying total DSBs in the *leu2::hisG* region (E) by DSBs in *HIS4::LEU2* region (G).
L: Interference is calculated as 1 – (observed double-cuts/expected double-cuts) = 1 – (A / J)
N: A one-tailed T-test was used to assess whether the observed frequency of double-cuts was less than expected (Is A < J ?). Interference is present in all *TEL1+* strains, and is lost in *sae2Δ tel1Δ* and *dmc1Δ tel1Δ*.
Q: A one-tailed T-test was used to assess whether interference in the test strain (*sae2Δ tel1Δ* or *sae2Δ rad24Δ*, or *dmc1Δ tel1Δ* or *dmc1Δ rad24Δ*) was lower than in the control strain (*sae2Δ* or *dmc1Δ*, respectively).
sae2Δ rad24Δ displayed moderately and significantly stronger interference (0.79 vs 0.68 for *sae2Δ*), possibly due to slightly lower lane background in these samples allowing more accurate (lower) double-cut measurement

Extended Data Figure 4 | Analysis of DSB interference between *HIS4::LEU2* and *leu2::hisG*. **a**, **b**, Agarose-embedded genomic DNA isolated at the indicated time points was fractionated by PFGE, transferred to nylon membrane and hybridized with probes recognizing **a**, the *FRM2* locus located between the *HIS4::LEU2* and *leu2::hisG* DSB hotspots, and **b**, the *CHA1* locus on the left telomere of chromosome III. Areas selected for quantification are indicated. **c**, Analysis of DSB interference between *HIS4::LEU2* and *leu2::hisG* regions. The frequency of DSB formation within *HIS4::LEU2* and *leu2::hisG* regions were measured in the various strains from PFGE using *CHA1* (**b**) and *FRM2* (**a**) probes, respectively, and the frequency of double-cuts were measured using the *FRM2* probe (**a**). Total DSBs arising within the *leu2::hisG* region were calculated by summing double-cuts and *leu2::hisG* DSBs. Standard deviation indicates the variation between repeat analyses ($n = 3$ for all samples except *rad24Δ dmc1Δ*: $n = 2$). See notes below table for further details.

©2015 Macmillan Publishers Limited. All rights reserved

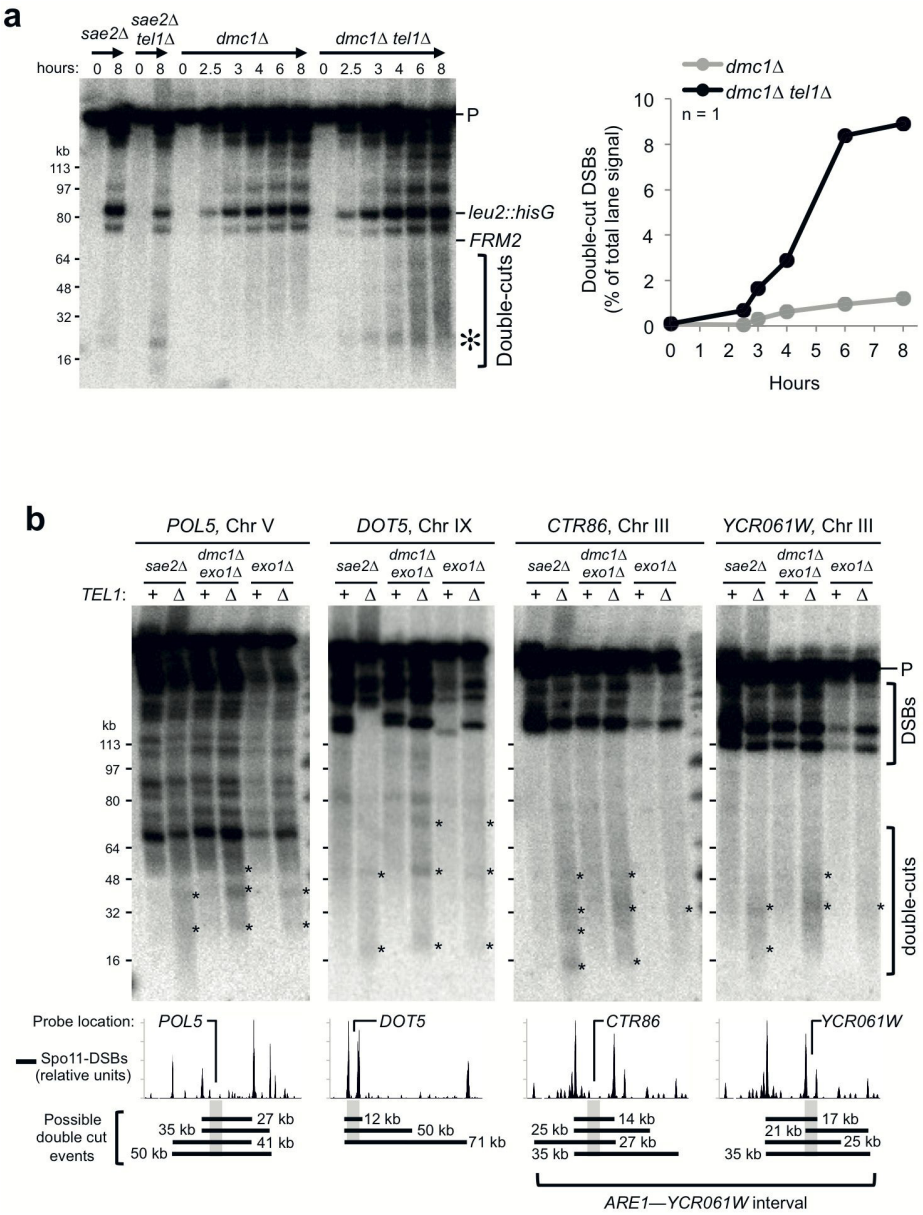

Extended Data Figure 5 | Analysis of DSB double-cutting at various genomic loci. **a**, **b**, Agarose-embedded genomic DNA isolated from the indicated time points and strains was fractionated by PFGE, transferred to nylon membrane and hybridized with various probes: *FRM2* (**a**); *POL5*, *DOT5*, *CTR86*, *YCR061W* (**b**). **a**, Detection of double-cut (left panel) and quantification (right panel). Major double-cut band corresponding to coincident DSBs at *HIS4*::*LEU2* and *leu2*::*hisG* is indicated with a star. **b**, Detection of double-cuts on different chromosomes following PFGE in strains fully (*dmc1*Δ *exo1*Δ and *sae2*Δ) or partially (*exo1*Δ) defective for DSB repair (top panel). Asterisks: *tel1*Δ-specific double-cut signals. Diagram depicts possible double-cuts (bottom panels).

©2015 Macmillan Publishers Limited. All rights reserved

a

Calculation using direct DSB measurement

*sae2*Δ										
COLUMN: A	**B**	**C**	**D**	**E**	**F**	**G**	**H**	**J**	**K**	**L**
	Observed double-cuts		Measured DSBs		Expected double-cuts		Interference		T-test: Observed vs Expected	
bp from *ARE1*	Average	StDev	Average	StDev	Average	StDev	Average	StDev	P-value	Interference?
-14501	0.037	0.024								
-9139	0.010	0.005								
-6162	0.013	0.009								
-5009	0.020	0.009	0.695	0.064	0.058	0.002	0.657	0.153	0.030	POSITIVE
-3723	0.033	0.000	0.710	0.042	0.060	0.007	0.436	0.069	0.037	POSITIVE
-2004	0.083	0.005	0.795	0.177	0.066	0.011	-0.284	0.278	0.170	no
-1220	0.140	0.028	2.830	1.047	0.234	0.073	0.352	0.322	0.230	no
-633	0.007	0.000	nd	nd						
***ARE1* DSB**			**8.366**	**0.525**						
1592	0.017	0.005	0.108	0.011	0.009	0.000	-0.851	0.459	0.148	no
2205	0.100	0.019	0.585	0.011	0.049	0.004	-1.064	0.552	0.064	no
3128	0.047	0.009	0.548	0.028	0.046	0.001	-0.022	0.218	0.901	no
4737	0.053	0.009	0.871	0.048	0.073	0.001	0.267	0.135	0.101	no
8496	0.007	0.000	0.419	0.087	0.035	0.005	0.806	0.028	0.016	POSITIVE
11638	0.007	0.000								
12585	0.010	0.005								
13398	0.027	0.019								
Total ± StDev	0.610	0.146	15.926	2.038						

Calculation using Spo11-oligo data (Pan et al. 2011)

*sae2*Δ										
A	**M**	**N**	**P**	**Q**	**R**	**S**	**T**	**U**	**V**
		Estimated DSBs		Expected double-cuts		Interference		T-test: Observed vs Expected	
bp from *ARE1*	Spo11-oligos	Average	StDev	Average	StDev	Average	StDev	P-value	Interference?
-14501	1087	1.603	0.101	0.134	0.017	0.736	0.142	0.041	POSITIVE
-9139	208	0.307	0.019	0.026	0.003	0.620	0.136	0.060	no
-6162	571	0.842	0.053	0.071	0.009	0.801	0.158	0.025	POSITIVE
-5009	665	0.981	0.062	0.082	0.010	0.748	0.146	0.024	POSITIVE
-3723	519	0.766	0.048	0.064	0.008	0.476	0.066	0.032	POSITIVE
-2004	874	1.289	0.081	0.108	0.014	0.226	0.053	0.135	no
-1220	1778	2.623	0.165	0.220	0.028	0.366	0.049	0.104	no
-633	163	0.240	0.015	0.020	0.003	0.667	0.042	0.017	POSITIVE
***ARE1* DSB**	**5672**	**8.366**	**0.525**						
1592	145	0.214	0.013	0.018	0.002	0.046	0.382	0.765	no
2205	838	1.236	0.078	0.104	0.013	0.016	0.305	0.844	no
3128	367	0.541	0.034	0.045	0.006	-0.050	0.339	0.884	no
4737	534	0.788	0.049	0.066	0.008	0.177	0.246	0.289	no
8496	138	0.204	0.013	0.017	0.002	0.606	0.049	0.020	POSITIVE
11638	319	0.471	0.030	0.039	0.005	0.830	0.021	0.011	POSITIVE
12585	266	0.392	0.025	0.033	0.004	0.685	0.183	0.035	POSITIVE
13398	5435	8.017	0.503	0.672	0.084	0.958	0.033	0.009	POSITIVE

*sae2*Δ *tel1*Δ										
COLUMN: A	**B**	**C**	**D**	**E**	**F**	**G**	**H**	**J**	**K**	**L**
	Observed double-cuts		Measured DSBs		Expected double-cuts		Interference		T-test: Observed vs Expected	
bp from *ARE1*	Average	StDev	Average	StDev	Average	StDev	Average	StDev	P-value	Interference?
-14501	0.200	0.019								
-9139	0.030	0.005								
-6162	0.070	0.005								
-5009	0.130	0.033	0.915	0.332	0.122	0.054	-0.111	0.221	0.882	no
-3723	0.233	0.009	1.170	0.212	0.155	0.041	-0.548	0.349	0.120	no
-2004	0.347	0.057	1.120	0.113	0.148	0.028	-1.416	0.830	0.047	NEGATIVE
-1220	1.543	0.052	3.570	0.184	0.469	0.016	-2.288	0.001	0.001	NEGATIVE
-633	0.163	0.071	nd	nd						
***ARE1* DSB**			**13.178**	**0.387**						
1592	0.143	0.052	0.254	0.071	0.033	0.002	-3.259	1.338	0.096	no
2205	0.750	0.042	1.350	0.047	0.180	0.066	-3.419	1.383	0.009	NEGATIVE
3128	0.400	0.038	0.841	0.057	0.112	0.036	-2.711	0.864	0.016	NEGATIVE
4737	0.583	0.061	1.603	0.255	0.213	0.052	-1.791	0.389	0.023	NEGATIVE
8496	0.050	0.005	0.500	0.000	0.066	0.006	0.241	0.007	0.092	no
11638	0.010	0.005								
12585	0.040	0.000								
13398	0.853	0.207								
Total ± StDev	5.547	0.660	24.500	1.658						
Fold increase	9.093		1.538							

*sae2*Δ *tel1*Δ										
A	**M**	**N**	**P**	**Q**	**R**	**S**	**T**	**U**	**V**
		Estimated DSBs		Expected double-cuts		Interference		T-test: Observed vs Expected	
bp from *ARE1*	Spo11-oligos	Average	StDev	Average	StDev	Average	StDev	P-value	Interference?
-14501	1087	2.525	0.215	0.334	0.057	0.397	0.046	0.087	no
-9139	208	0.483	0.041	0.064	0.011	0.530	0.006	0.056	no
-6162	571	1.327	0.113	0.175	0.030	0.597	0.042	0.039	POSITIVE
-5009	665	1.545	0.132	0.204	0.035	0.368	0.054	0.159	no
-3723	519	1.206	0.103	0.159	0.027	-0.480	0.192	0.068	no
-2004	874	2.031	0.173	0.269	0.046	-0.328	0.436	0.268	no
-1220	1778	4.131	0.352	0.546	0.093	-1.858	0.391	0.006	NEGATIVE
-633	163	0.379	0.032	0.050	0.009	-2.187	0.870	0.153	no
***ARE1* DSB**	**5672**	**13.178**	**1.124**						
1592	145	0.337	0.029	0.045	0.008	-2.164	0.626	0.117	no
2205	838	1.947	0.166	0.257	0.044	-1.941	0.335	0.008	NEGATIVE
3128	367	0.853	0.073	0.113	0.019	-2.570	0.273	0.011	NEGATIVE
4737	534	1.241	0.106	0.164	0.028	-2.575	0.234	0.013	NEGATIVE
8496	138	0.321	0.027	0.042	0.007	-0.187	0.091	0.338	no
11638	319	0.741	0.063	0.098	0.017	0.892	0.066	0.019	POSITIVE
12585	266	0.618	0.053	0.082	0.014	0.503	0.084	0.051	no
13398	5435	12.627	1.077	1.670	0.284	0.471	0.214	0.082	no

Notes:

A-V	Column identifiers
A	Distance (in bp) of test DSB from *ARE1*-DSB (This equals the length of double-cut assayed.)
B-J & N-T	Values (reported as % of lane signal) are the average and standard deviation of two independent repeats. Individual values from each repeat were averages of the 6-10 h timepoints.
B & C	Average and standard deviation of observed double-cut frequencies as measured by Southern blotting using *ARE1* and *BUD23* probes
D & E	Average and standard deviation of single-cut DSB frequencies as measured by Southern blotting using various AseI, BglII, and NgoMIV digests and *TAF2*, *RSC6* and *PWP2* probes (Extended Data Table 2)
F & G	Average and standard deviation of expected double-cut frequencies calculated by multiplying % DSBs at *ARE1* by the measured single-cut DSB frequency at each site (D)
H & J	Average and standard deviation of interference calculated by the formula: 1–(B/F). These values are plotted in Figure 4
K & L	2-tailed T-test between the observed and expected datasets (B and F). Rows with P-values below 0.05 are coloured according to the type of (significant) interference: Red=Positive Blue=Negative Clear=Not significantly different from independence
M	Relative Spo11-oligo counts obtained from Pan et al, Cell 2011. Qualitatively similar results were obtained using Spo11-oligo counts from a second WT dataset (Thacker et al., Nature 2014) and from an unpublished *tel1*Δ dataset (S.Keeney and N.Mohibullah, pers. comm.)
N & P	Average and standard deviation of single-cut DSB frequencies as estimated by converting Spo11-oligo counts to DSB frequencies using the frequency of DSBs measured at *ARE1* (highlighted in yellow)
Q & R	Average and standard deviation of expected double-cut frequencies calculated by multiplying % DSBs at *ARE1* by the single-cut DSB frequencies estimated from the converted Spo11-oligo counts (N)
S & T	Average and standard deviation of interference calculated by the formula: 1–(B/Q). These values are plotted in Figure 4
U & V	2-tailed T-test between the observed and expected datasets (B and Q). Rows with P-values below 0.05 are coloured according to the type of (significant) interference: Red=Positive Blue=Negative Clear=Not significantly different from independence
nd	Not determined (DSB frequency could not be assessed directly at this site due to contamination from strong flanking DSB peaks at *ARE1*)
Total ± StDev	Refers to the aggregated frequency of double-cuts (B) or DSBs (D) observed across the *ARE1* region
Fold increase	Refers to the aggregated increase in frequency of double-cuts (B) or DSBs (D) observed across the *ARE1* region in *sae2*Δ *tel1*Δ compared to *sae2*Δ

b

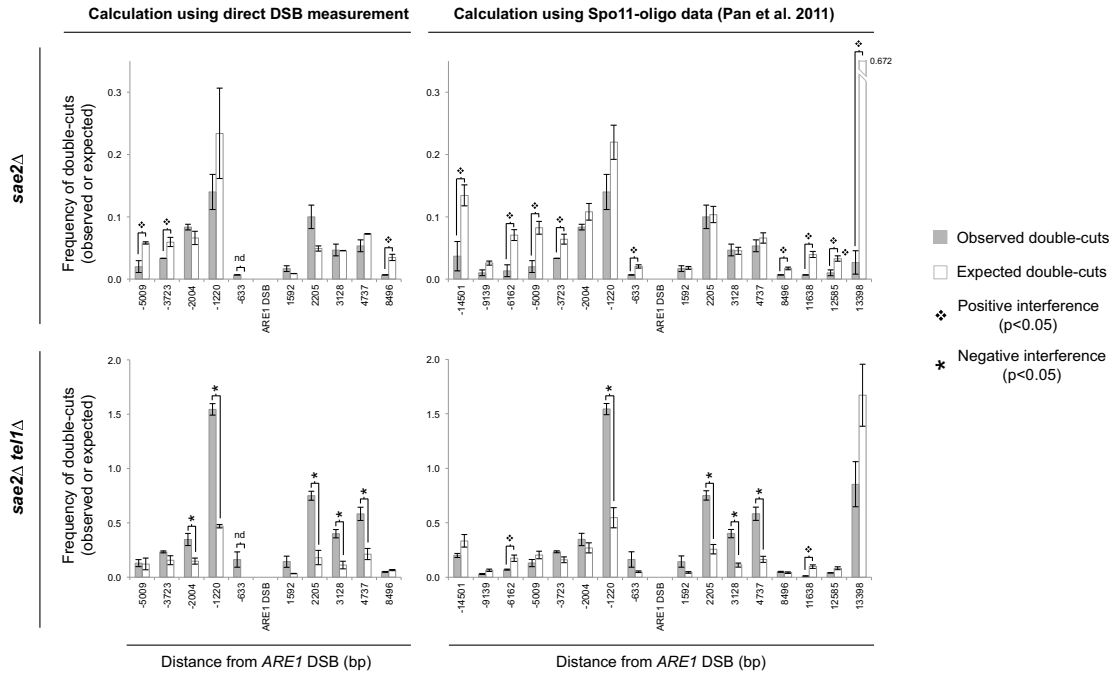

Extended Data Figure 6 | Analysis of DSB interference across the *ARE1* region. **a**, DSB interference was calculated in *sae2Δ* (top) and *sae2Δ tel1Δ* (bottom) using the following formula: 1–f(observed double-cuts)/f(expected double-cuts), where the expected double-cut values were calculated using two methods. Left, single-cut frequencies were measured by Southern-blot using a *TAF2* probe (for DSB sites on the left of *ARE1*) or a *PWP2* and *RSC6* probe (for the right-hand side of *ARE1*; Extended Data Table 2). Right, calculations were made after converting the measured Spo11-oligo frequency[1] at each DSB site to a % DSB ± s.d. value by using the measured DSB frequency at *ARE1* in *sae2*Δ or *sae2*Δ *tel1*Δ for normalization (see Notes below table and Methods for further details). **b**, Chart of observed (column B) and expected (column F and Q) frequencies of double-cuts. Error bars, s.d. $n = 2$. *P* values, two-tailed *t*-test. Double-cut products that were present at a frequency that was statistically different from that for no interference (independence) were highlighted in **a** according to the type of interference present: red indicates positive DSB interference, blue indicates negative DSB interference (concerted DSB formation); in **b** the same statistical differences were indicated with open diamonds or asterisks, respectively.

©2015 Macmillan Publishers Limited. All rights reserved

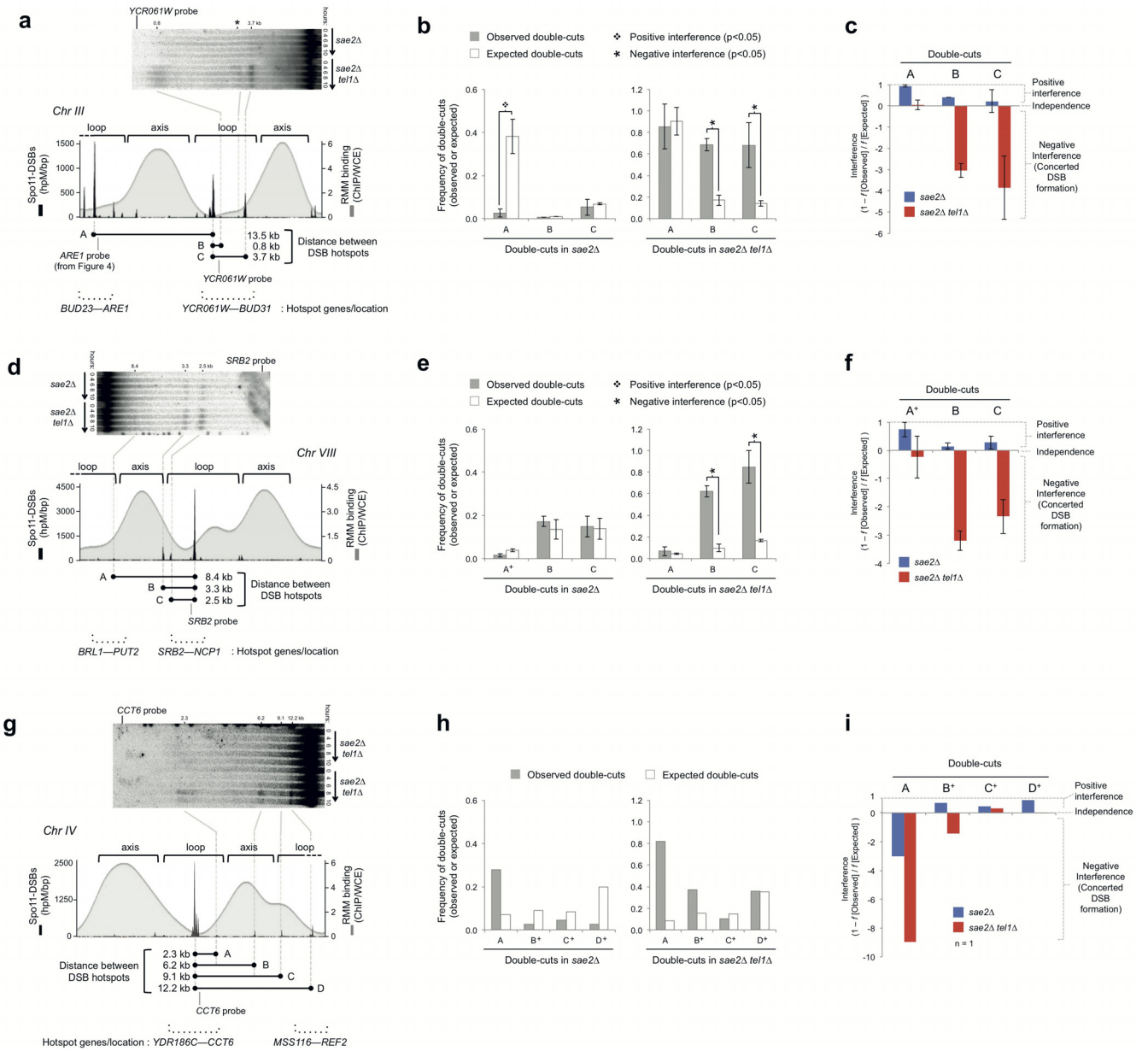

Extended Data Figure 7 | Tel1 suppresses concerted DSB formation within chromatin loop domains at numerous chromosomal loci. **a**–**i**, DSB interference was calculated across three DSB hotspot regions located on three different chromosomes: chromosome III, *BUD23–ARE1* to *YCR061W–BUD31* (**a**–**c**); chromosome VIII, *BRL1–PUT2* to *SRB2–NCP1* (**d**–**f**); and chromosome IV, *YDR186C–CCT6* to *MSS116–REF*[2] (**g**–**i**). **a**, **d**, **g**, Upper panels, genomic DNA isolated from *sae2*Δ or *sae2*Δ *tel1*Δ strains at the indicated time points was fractionated by agarose electrophoresis, transferred to nylon membrane and hybridized with the indicated probes: *YCRO61W* (**a**), *SRB2* (**d**), *CCT6* (**g**). Lower panels, diagram of mean RMM binding profile[14] overlaid with Spo11-DSB hotspot peaks[1]. Intervals between various detectable double-cut events are indicated below and specified with the letters A to D. Probes used for detecting double-cuts by Southern blotting are indicated. **b**, **e**, **h**, Chart of observed and expected double-cuts for each of the indicated intervals, calculated as an average (per repeat) across the 4–10 h time points. Expected double-cut frequencies for each interval were calculated by multiplying the DSB frequencies (average across 4–10 h) at the two sites. Single-cut frequencies were measured by Southern-blot (see Extended Data Table 2 and Methods for details). For some intervals (superscript with a "+"), due to no Southern DSB data being available at the minor DSB site, calculations were made using the normalized Spo11-oligo frequency[1] at the minor DSB site (as was performed in Fig. 4 and described in Methods). Asterisks and open diamonds indicate significant negative and positive interference, respectively. **c**, **f**, **i**, DSB interference was calculated by the following formula: 1 – *f*(observed double-cuts)/*f*(expected double-cuts). Values above zero indicate positive DSB interference. Values below zero indicate negative DSB interference (concerted DSB formation). Conclusion: In addition to *ARE1* (Fig. 4), at all three additional loci tested, concerted DSB formation is localized predominantly within a domain approximately demarcated by the RMM binding profile (see **a**, **d** and **g**, lower panels). Notably, coincident formation of two DSBs, one within the *BUD23-ARE1* domain and one within the *YCR061W-BUD31* domain, arise independently in *sae2*Δ *tel1*Δ despite coincident DSB formation within each interval displaying negative interference. In **a**, double-cuts in interval A were measured using the *ARE1* probe (Fig. 4a). Asterisk in **a** upper panel denotes a band that is a mixture of two *tel1*Δ-dependent double-cuts, which owing to the relative location of the *YCR061W* probe and DSB sites cannot be unambiguously assigned and therefore were not analysed. Error bars, s.d. $n = 2$, except **g**–**i** where only one experiment was performed. *P* values, two-tailed *t*-test.

©2015 Macmillan Publishers Limited. All rights reserved

a

COLUMN:	a	b	c	d	e	f	g	h	i
Tethering frequency		DSB	Measured frequency of DSB formation (population average)	Expected double-cutting frequency of A x B within population (using population average DSB frequencies) i.e. column c: [A x B]	DSB	DSB frequency within the tethered loop i.e. [c/a]	Expected double-cutting frequency of A x B within tethered loop (using the DSB frequencies within the tethered loop) i.e. column f: [A x B]	Corrected expected double-cutting frequency of A x B within population (using the double-cut frequencies within the tethered loop) i.e. [g x a]	Apparent interference i.e. 1–[h/d]
All the time:	1.00	A	0.10	0.005	A	0.10	0.005	0.005	0.0
		B	0.05		B	0.05			
Half the time: (see "b" below)	0.50	A	0.10	0.005	A	0.20	0.020	0.010	-1.0
		B	0.05		B	0.10			
1/4 of the time:	0.25	A	0.10	0.005	A	0.40	0.080	0.020	-3.0
		B	0.05		B	0.20			
1/5th of the time: (see "c" below)	0.20	A	0.10	0.005	A	0.50	0.125	0.025	-4.0
		B	0.05		B	0.25			
1/6th of the time:	0.167	A	0.10	0.005	A	0.60	0.180	0.030	-5.0
		B	0.05		B	0.30			

b

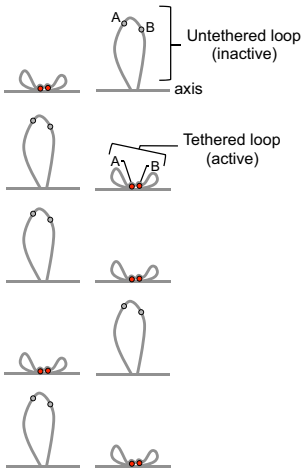

In this worked example, 50% of chromatids in the population are active/tethered at this locus

Observed population average DSB frequencies: A = 0.1, B = 0.05
Expected double-cut frequency: A x B = 0.005
Probability of loop tethering: 0.5 (i.e. on average 50% of loops tether/prime)
Probability of DSB formation per tethered loop: A* = 0.2, B* = 0.1
Probability of double-cut per tethered loop: A* x B* = 0.02
Observed population average double-cut frequencies: (A* x B*) x 0.5 = 0.01
If DSBs form independently, apparent interference: 1 – (0.01 / 0.005) = -1

Thus, loss of an interference signal, within a loop domain that is active/tethered in only a subpopulation of chromosomes will result in observed negative interference proportional to: 1 – (1 / loop tethering frequency) = 1 – (1 / 0.5), in this example.

c

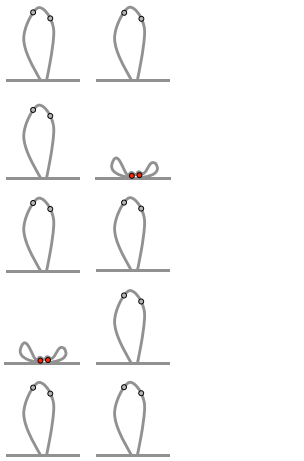

In this worked example, 20% of chromatids in the population are active/tethered at this locus

Observed population average DSB frequencies: A = 0.1, B = 0.05
Expected double-cut frequency: A x B = 0.005
Probability of loop tethering: 0.2 (i.e. on average 20% of loops tether/prime)
Probability of DSB formation per tethered loop: A* = 0.5, B* = 0.25
Probability of double-cut per tethered loop: A* x B* = 0.125
Observed population average double-cut frequencies: (A* x B*) x 0.20 = 0.025
If DSBs form independently, apparent interference: 1 – (0.025 / 0.005) = -4.0

Thus, loss of an interference signal, within a loop domain that is active/tethered in only a subpopulation of chromosomes will result in observed negative interference proportional to: 1 – (1 / loop tethering frequency) = 1 – (1 / 0.20), in this example.

Extended Data Figure 8 | Stochastic loop tethering (activation) predicts apparent short-range negative interference. **a**, In this model, DSBs A and B reside within a single loop domain (subject to tethering-dependent DSB formation), which is active in only a subpopulation of cells. The expected frequency of coincident DSB formation (double-cutting), assuming no DSB interference, is calculated for different frequencies of loop activation/tethering per chromatid assuming a model where DSB formation is wholly dependent on loop activation/tethering. In summary, loop activation/tethering at a frequency of X, will result in apparent negative interference of $1 - 1/X$. See text for further details. **b**, **c**, Cartoons (left) and worked examples (right) for situations in which 50% (**b**) or 20% (**c**) of the chromatids within the assayed population are active/tethered at the test locus. The cartoons depict the tethering state of an average sample of 10 chromatids from the population. It is also possible that loop tethering and loop activation are not synonymous processes. In principle, activation of a loop might precede and enable tethering, but not be caused by it.

©2015 Macmillan Publishers Limited. All rights reserved

Extended Data Table 1 | Table of strains used in this study

Strains	Genotype	Reference
SG147	*MATa/alpha, ho::LYS2/", lys2/", ura3/", arg4-nsp/", leu2::hisG/", his4X::LEU2/", nuc1::LEU2/", dmc1Δ::LEU2/"*	Gray et al, 2013
SG343	*MATa/alpha, ho::LYS2/", lys2/", ura3/", arg4-nsp/", leu2::hisG/", his4X::LEU2/", nuc1::LEU2/", dmc1Δ::HphMX/", tel1Δ::HphMX/",*	This study
MJ781	*MATa/alpha, ho::LYS2/", lys2/", ura3/", arg4-nsp/", leu2::hisG/", his4X::LEU2/", nuc1::LEU2/", dmc1Δ::LEU2/", rad24Δ::Hyg/"*	Gray et al, 2013
MJ315	*MATa/alpha, ho::LYS2/", lys2/", ura3/", arg4-nsp/", leu2::hisG/", his4X::LEU2/", nuc1::LEU2/", sae2Δ::KanMX6/"*	Gray et al, 2013
SG346	*MATa/alpha, ho::LYS2/", lys2/", ura3/", arg4-nsp or bgl?/", leu2::hisG or leu2Δ?/", his4X::LEU2/", nuc1::LEU2/", tel1Δ::HphMX4/", sae2Δ::KanMX6*	This study
SG103	*MATa/alpha, ho::LYS2/", lys2/", ura3/", arg4-nsp/", leu2::hisG/", his4X::LEU2/", nuc1::LEU2/", rad24Δ::Hyg/", sae2Δ::KanMX/",*	Gray et al, 2013
VG402	*MATa/alpha, ho::LYS2/", lys2/", ura3/", arg4-nsp/", leu2::hisG,/" his4X::LEU2/", nuc1::LEU2/", sae2Δ::KanMX4/", tel1Δ::HphMX4/"*	This study
MJ6	*MATa/alpha, ho::LYS2/"', lys2/'', ura3/'', arg4-nsp/'', leu2::hisG/'', his4X::LEU2/'', nuc1::LEU2/''*	Neale et al, 2005
SG344	*MATa/alpha, ho::LYS2/", lys2/", ura3/", arg4-nsp/", leu2::hisG/", his4X::LEU2/", nuc1::LEU2/", tel1Δ::HphMX4*	This study
VG392	*MATa/alpha, ho::LYS2/", lys2/", ura3/", arg4-nsp/", leu2::hisG/", his4X::LEU2/", nuc1::LEU2/", exo1Δ::KanMX4/"*	This study
VG393	*MATa/alpha, ho::LYS2/", lys2/", ura3/", arg4-nsp/", leu2::hisG,/" his4X::LEU2/", nuc1::LEU2/", exo1Δ::KanMX4/", tel1Δ::HphMX4/"*	This study
VG376	*MATa/alpha, ho::LYS2/", lys2/", ura3/", arg4-nsp/", leu2::hisG/", his4X::LEU2/", nuc1::LEU2/", dmc1Δ::HphMX4/", tel1Δ::HphMX4/", exo1Δ::KanMX4/"*	This study
VG377	*MATa/alpha, ho::LYS2/", lys2/", ura3/", arg4-nsp/", leu2::hisG/", his4X::LEU2/", nuc1::LEU2/", dmc1Δ::HphMX4/", exo1Δ::KanMX4/"*	This study

All strains are of the SK1 background. Genetic modifications were generated by transformation or intercrossing using standard methods. Laboratory origin of strains is indicated.

©2015 Macmillan Publishers Limited. All rights reserved

Extended Data Table 2 | Table of primers/probes used in this study for DSB and double-cut detection

Probe	ORF chromosome coordinates	primers	Digestion	Comments
Figure 1 and Extended Data Figure 1				
RMD6	L ChrV: 13720 to 14415	RMD6_F@+13 CTTGCAACATCGTTATACTCCCAG RMD6_R@+592 GAACTTTGAACCTTTGCACCTCTAC	NA	
YER186C	R ChrV: 562625 to 561705	YER186C_F@+4 TGTGGCATCCTGATGGTTACGAGC YER186C_R@+674 TCCTCTATGCTATCACCCACCTCTG	NA	
FIR1	R ChrV: 215063 to 217693.	FIR1_F@+1 ATGAGCCTCCCTGTTACACCTGTCAA FIR1_R@+944 ATTCCAAGAAGCTTATCAGCATCTGC	NA	
CHA1	L ChrIII: 16880 to 15798	CHA1_F@-9 ACCAGCGAGATGTCGATAGTCTAC CHA1_R@+1052 TCTGGAAATATGAAATTGTCAGCG	NA	Also Extended Data Figure 3 & 4
GIT1	R ChrIII: 298605 to 297049	GIT1_F@+35 GGAAGTGAACGAGAACACTAATCC GIT1_R@+891 AACGGAACTGATAATTGTTGAACTG	NA	Also Extended Data Figure 3
SYP1	R ChrIII: 176438 to 173826	SYP1_F@+1016 ACACCCTAAGATCTAAAGTGGGCTC SYP1_R@+1754 GGATTTAGTTCTCTTAGCTCGCCAG	NA	Also Extended Data Figure 3
CBP2	L ChrVIII: 25509 to 23617	CBP2_F@+712 CGCCACTTTGCACCTTGAATGAA CBP2_R@+1356 TTTCGATTTTGTCAGCACGGTTTG	NA	
CRG1	R ChrVIII: 519437 to 520312	CRG1_F@+177 TTTAAGGAAGTGATTGGGATTGAT CRG1_R@+749 GGATTATCTCTAGCCCAAGAAGTG	NA	
CIC1	ChrVIII: 210848 to 211978	CIC1_F@+476 CTTAAAGACCGTTTACAAGGCATATGAG CIC1_R@+1116 CTTGACAGCTTCTGACTCGCTAGATTC	NA	
JEN1	L ChrXI:22234 to 24084	JEN1_F@-2 ATATGTCGTCGTCAATTACAGATGAG JEN1_R@+620 GGCCACTTTCTGGAAGACTTATC	NA	
SIR1	R ChrXI: 640540 to 642504	SIR1_F@+14 CTCCAGGCTTGCAGTTATTGATG SIR1_R@+581 CATTTTGTTAAGCCAACCTGACTC	NA	
NUP100	ChrXI: 310199 to 313078	NUP100_F@+128 ATTCCACCAGTAACAATGCCCAATCAG NUP100_R@+895 GAGTGCTGCTGTTCATCGAGTTTTGTC	NA	
Figure 2 and Extended Data Figure 4 & 5				
FRM2	L ChrIII: 75285 to 74704	FRM2_F@+27 GCTATTACAAACCGTCGTACCATC FRM2_R@+645 CATCGCTGAGGTATCATTACTTCAT	NA	Figure 2a, b, and e, Extended Data Figure 4a & 5a
POLV	L ChrV: 51539 to 48471	POL5_F@+1 ATGACAGGGAAAGTCAACAGAGACCT POL5_R@+900 ACCAAACAACGGTAGCAGAACACTC	NA	Extended Data Figure 5b
DOT5	R ChrIX: 334882 to 335529	DOT5_F@+1 ATGGGTGAAGCACTACGTAGATCAAC DOT5_R@+882 AATAGTGCCCGTTCTCAATGTAAACC	NA	Extended Data Figure 5b
YCR061W (I)	R ChrIII: 225563 to 227458	YCR061W_F@+58 CCCATGATGACATGGACATGGAC YCR061W_R@+884 GGTATGTCTTGAGGAAGCAGAGG	NA	Extended Data Figure 5b Also Extended Data Figure 7a
CTR86	R ChrIII: 220067 to 218376	CTR86_F@+50 TACCATGATGAAGAACGACCCATGTTG CTR86_R@+898 ATTGCAATATCTGCAACAAAGTGGTG	NA	Extended Data Figure 5b
Figure 3				
Leu2		LEU2_F ATATACCATTCTAATGTCTGC LEU2_R AAGGATTTTCTTAACTTCTTCGGCG	NA	Central probe
Leu2LH		LEU2LH_F GTACGTACAGACCGTCCTGACGG LEU2LH_R CTTTGTCGGAAGCCTTCACCACGTCC	*Pst*I	Left probe
MRX2	ChrIII: 63282 to 62776	HIS4_F@+5170 CGTGAAGTGGAACGATGCCC HIS4_R@+5493 GCAACTGTTTCCAGCCTTCACC	*Pst*I	Right probe
Figure 4				
BUD23	R ChrIII: 211545 to 210718	BUD23_F@+1 ATGTCACGTCCTGAGGAGTTGG BUD23_R@+800 GTGAACTTGGAGTCCTTCGCAAC	NA	Quantification of DC between *ARE1* and hotpots on the left of *ARE1*
ARE1	R ChrIII: 211929 to 213761	ARE1_F@+54 ACTCAATTCCGCAGAAGCCA ARE1_R@+715 TTGCCAAGTCCAACATTGCG	NA	Quantification of DC between *ARE1* and hotpots on right of *ARE1*
TAF2	R ChrIII: 205397 to 201174	TAF2_F@+23 CCACTCCTAGAGCCATTGTTAG TAF2_R@+693 TCATCAAGCAAATCGACACATGG	*Ase*I *Ngo*MIV	Quantification of DSB% at *ARE1* and hotspots on the left of *ARE1*
PWP2	R ChrIII: 223228 to 220457	PWP2_F@+35 GTACGGTCTACAGGCAAGGTAAC PWP2_R@+815 TTGCTGGATGGAAGGTGACACAC	*Ngo*MIV	Quantification of DSB% at *ARE1* and hotspots on the right of *ARE1*
RSC6	R ChrIII: 214994 to 216445		*Bgl*II	Quantification of DSB% at *ARE1* and hotspots on the right of *ARE1*
CTR86	R ChrIII: 220067 to 218376	CTR86_F@+50 TACCATGATGAAGAACGACCCATGTTG CTR86_R@+898 ATTGCAATATCTGCAACAAAGTGGTG	*Bgl*II	Quantification of DSB% at *YCR054W*
YCR061W (I)	R ChrIII: 225563 to 227458	YCR061W_F@+58 CCCATGATGACATGGACATGGAC YCR061W_R@+884 GGTATGTCTTGAGGAAGCAGAGG	*Bgl*II	Quantification of DSB% at *YCR061W*
YCR061W (II)	R ChrIII: 225563 to 227458	YCR061W_F@+1283 GGTCCACCAACATCTTCTTGGAG YCR061W_R@+2176 TCAGAGAGAACCTCCAGTAGAGTC	*Bgl*II *Pst*I *Eco*RI	Quantification of DSB% at *YCR061W*
Extended Data Figure 7				
YCR061W (I)	R ChrIII: 225563 to 227458	YCR061W_F@+58 CCCATGATGACATGGACATGGAC YCR061W_R@+884 GGTATGTCTTGAGGAAGCAGAGG	NA	Quantification of DC between *YCR061W* and *YCR065W*
YCR061W (II)	R ChrIII: 225563 to 227458	YCR061W_F@+1283 GGTCCACCAACATCTTCTTGGAG YCR061W_R@+2176 TCAGAGAGAACCTCCAGTAGAGTC	*Pst*I *Eco*RI	Quantification of DC between *YCR061W* and *YCR065W* DSB% at *YCR061W* and weak hotspot within *YCR061W* DSB% at *YCR063W* and *YCR065W*
PUT2	R ChrVIII: 181977 to 183704	PUT2_F@+1 ATGCTATCAGCAAGGTGCCTC PUT2_R@+989 GCACTTGGGTGAACTAGATGG	*Stu*I	Quantification of DSB% at *YHR039W, YHR040W* and *YHR042W*
SRB2	R chrVIII: 189131 to 189864	NCP1_F@-512 TTCCTTCGCTCAATTGCACTTTCCC NCP1_R@-56 CCACTACAGGAACGCAAACTTAAGC	NA	Quantification of DC between *SRB2/NCP1* and *YHR039W, YHR040W* and *YHR042W*.
CCT6	R ChrIV: 836421 to 838061	CCT6_F@+20 TCCGAAGGCTGAATCGTTGAG CCT6_R@+1025 CTTCCACAGAGTTCTGAGCTTC	*Pst*I	Quantification of DC between *CCT6* and *SLY1* DSB% at *CCT6*
SLY1	ChrIV: 838392 to 840392	SLY1_F@+1 ATGGCTGTGGAGGAAATTGCGTCC SLY1_R@+1025 TTCTCTGCAGCTTCTGGGAATGGC	*Eco*RI	DSB% at *SLY1*

Indicated columns: location of probes (gene locus) for Southern blots, primer sequences used to generate these probes (by PCR), and reference to figure(s) within this manuscript in which probes were used for data collection. For quantification of PFGE and double-cuts (DC), no DNA digestion was performed before electrophoresis. For quantification of single-cut DSB frequencies at specific loci, DNA was first digested to completion with the indicated restriction enzyme before electrophoresis.

©2015 Macmillan Publishers Limited. All rights reserved